

Structure of LARP7 protein p65–telomerase RNA complex in telomerase revealed by cryo-EM and NMR

Yaqiang Wang^{1,2,3,4}, Yao He^{1,2,3,4}, Yanjiao Wang^{1,2,3,4}, Yuan Yang^{1,2,3,4}, Mahavir Singh¹, Catherine D. Eichhorn¹, Xinyi Cheng¹, Yi Xiao Jiang¹, Z. Hong Zhou^{2,3}, and Juli Feigon^{1,*}

¹ Department of Chemistry and Biochemistry, University of California Los Angeles, Los Angeles, CA 90095-1569 USA

² Department of Microbiology, Immunology, and Molecular Genetics, University of California Los Angeles, Los Angeles, CA 90095, USA

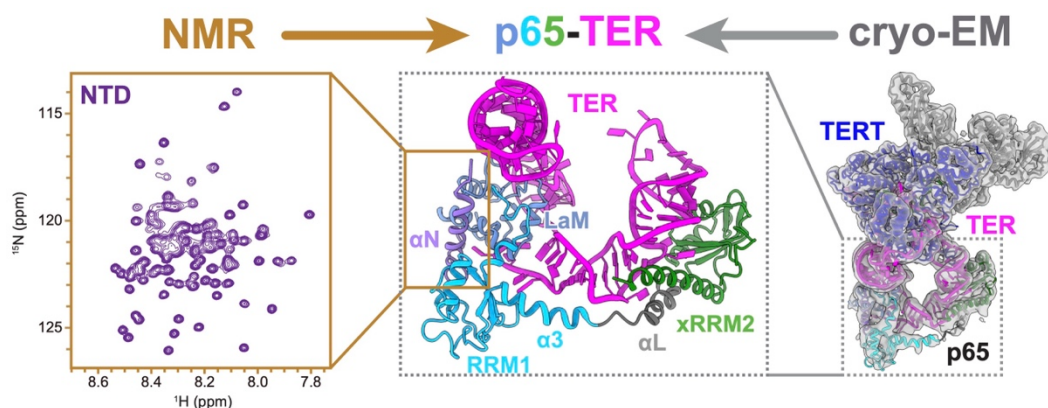
³ California NanoSystems Institute, University of California Los Angeles, Los Angeles, CA 90095, USA

Equal contribution

* To whom correspondence should be addressed. Tel: +1 310 206 6922; Email: feigon@mbi.ucla.edu

Present Address: Mahavir Singh, Molecular Biophysics Unit, Indian Institute of Science, Bengaluru, 560012, India; Catherine D. Eichhorn, Department of Chemistry, University of Nebraska, Lincoln, NE 68508 USA

GRAPHICAL ABSTRACT



HIGHLIGHTS

- Structure of LARP7 p65 bound to telomerase RNA in telomerase solved by cryoEM and NMR
- p65 interacts extensively with and refolds TER for telomerase assembly
- Full-length p65 structure provides new insights into chaperone activity of LARP7
- A previously unobserved helix in p65 N-terminal IDR interacts with the La module

1 **ABSTRACT**

2 La-related protein 7 (LARP7) are a family of RNA chaperones that protect the 3'-end of RNA and are
3 components of specific ribonucleoprotein complexes (RNP). In *Tetrahymena thermophila* telomerase,
4 LARP7 protein p65 together with telomerase reverse transcriptase (TERT) and telomerase RNA
5 (TER) form the core RNP. p65 has four known domains—N-terminal domain (NTD), La motif (LaM),
6 RNA recognition motif 1 (RRM1), and C-terminal xRRM2. To date, only the xRRM2 and LaM and their
7 interactions with TER have been structurally characterized. Conformational dynamics leading to low
8 resolution in cryo-EM density maps have limited our understanding of how full-length p65 specifically
9 recognizes and remodels TER for telomerase assembly. Here, we combined focused classification of
10 *Tetrahymena* telomerase cryo-EM maps with NMR spectroscopy to determine the structure of p65–
11 TER. Three previously unknown helices are identified, one in the otherwise intrinsically disordered
12 NTD that binds the La module, one that extends RRM1, and another preceding xRRM2, that stabilize
13 p65–TER interactions. The extended La module (α N, LaM and RRM1) interacts with the four 3'
14 terminal U nucleotides, while LaM and α N additionally interact with TER pseudoknot, and LaM with
15 stem 1 and 5' end. Our results reveal the extensive p65–TER interactions that promote TER 3'-end
16 protection, TER folding, and core RNP assembly and stabilization. The structure of full-length p65
17 with TER also sheds light on the biological roles of genuine La and LARP7 proteins as RNA
18 chaperones and core RNP components.

19

20 **KEYWORDS**

21 La protein, La module, RRM, telomerase, pseudoknot

22

23 **INTRODUCTION**

24 The eukaryotic genuine La and La-related protein (LARP) superfamily comprise a diverse class of
25 RNA binding proteins with various functions in RNA metabolism.¹⁻³ Genuine La protein binds nascent
26 RNA polymerase III transcripts at their 3'-polyuridine (polyU) tail via its La module, which comprises a
27 La motif (LaM) and an RNA recognition motif (RRM1).⁴ Most genuine La proteins also have a C-
28 terminal atypical RRM2 that has RNA folding and chaperone activity.^{5,6} Although all LARP families
29 contain a similar La module, their C-terminal domain structures diverge significantly depending on the
30 cognate RNA and function. LARPs bind to specific RNAs to function in folding, assembly, and
31 biogenesis of ribonucleoproteins (RNP). Among LARPs, La-related protein 7 (LARP7) members are
32 the closest relatives to genuine La protein.⁷

33 All LARP7 identified to date are components of 7SK or telomerase RNPs. Larp7 (a specific protein
34 in metazoa) is an essential component of 7SK RNP and required for the sequestration of positive
35 transcription elongation factor b (P-TEFb), which regulates the transition of RNA polymerase II from
36 promoter proximal paused to productive elongation.⁸⁻¹⁰ Telomerase is essential for the maintenance of
37 telomeric DNA at linear chromosome ends in most eukaryotes. Telomerase comprises a noncoding
38 RNA (telomerase RNA, TER), telomerase reverse transcriptase (TERT), and species-specific
39 associated proteins.^{11,12} The size of TER varies among species, but it has two evolutionarily
40 conserved domains, template/pseudoknot (t/PK) and stem-terminus element (STE), that
41 independently bind TERT and are required for telomerase activity.¹³ Ciliate TERs, like metazoan 7SK
42 RNA, are synthesized by RNA polymerase III. LARP7 proteins p65 and p43 in *Tetrahymena*
43 *thermophila* and *Euplotes aediculatus*, respectively, and Pof8 in *Schizosaccharomyces pombe*
44 (fission yeast) are constitutive components of telomerase¹⁴⁻²⁰ that bind TER and are required for its
45 biogenesis.

46 In *Tetrahymena* telomerase holoenzyme, p65 is required for TER accumulation *in vivo*²¹ and is an
47 essential component of the core RNP.¹² Biochemical, single-molecule, and structural studies showed
48 that p65 initiates hierarchical assembly of telomerase through its interactions with TER stem 4.²²⁻²⁵
49 *Tetrahymena* p65 has four known domains: N-terminal domain (NTD), LaM, RRM1, and a C-terminal
50 xRRM2 (Figure 1A).^{23,26} The LaM and RRM1 comprise the La module, which is highly conserved in
51 sequence among LARP7s and genuine La.¹ Crystal structures of La modules of human Larp7 and
52 human genuine La protein show conserved interactions with RNA UUU-3'-OH in a V-shaped

53 configuration.^{4,27} However, to date, most structural studies of p65 were focused on its xRRM2
54 interaction with TER stem-loop 4 (SL4, STE in *Tetrahymena* TER). xRRMs have an atypical mode of
55 RNA recognition divergent from that of canonical RRM^s.^{25,28,29} In *Tetrahymena* telomerase, p65
56 xRRM2 specifically recognizes and bends SL4 to promote telomerase assembly.^{25,30} However, since
57 TER stem 1 (S1) and SL4 are connected by a single-stranded linker (Figure 1B), knowledge of the
58 xRRM2–S4 structure²⁵ outside the context of the entire core RNP does not completely explain how
59 p65 positions loop 4 of TER for interaction with TERT, where it is inserted between TRBD and CTE,
60 during telomerase RNP assembly.³¹⁻³³

61 We previously reported a 3.3 Å overall resolution cryo-EM structure of *Tetrahymena* telomerase
62 with DNA bound at the second step of telomere repeat synthesis.³⁴ While high resolution features of
63 the TERT–TER catalytic core could be clearly discerned, the p65–TER region has a much lower
64 resolution due to conformational dynamics and its location at the periphery of the core RNP. Globally,
65 the structure shows that p65 and TER form a U-shape structure under TERT,³¹⁻³³ and p65 LaM and
66 xRRM2 bind near the two ends of the U, respectively.³⁴ However, the structure of the rest of p65
67 (NTD, RRM1, and linker between RRM1 and xRRM2) and interactions with TER have not been
68 determined. Here we report another cryo-EM reconstruction of *Tetrahymena* telomerase with
69 improved local resolution of p65–TER obtained by focused classification on a larger dataset (Figure
70 1C). Although the resolution in parts of the cryo-EM map is not sufficient for *de novo* model building,
71 by integrating information from NMR studies and Rosetta modeling, we were able to build a model of
72 full-length p65 bound to TER in the telomerase holoenzyme. We find that almost all of p65, including
73 a helix in the otherwise unstructured NTD, interacts with TER, thereby linking stem 1 and stem 4 that
74 close the catalytically essential t/PK and STE, respectively, as well as the PK. This structure of the
75 complete p65–TER complex also sheds light on how genuine La and other Larp7 proteins may
76 chaperone their RNA partners.

77 RESULTS

78 Overall structure of p65–TER in telomerase

79 To obtain a model of p65–TER in telomerase, we combined telomerase particles from two different
80 cryo-EM datasets, and performed focused classification on the p65 La module (LaM and RRM1)
81 (Figure S1A). An additional round of focused classification on p65 LaM was performed to further

82 improve densities at its interfaces with TER S1, PK and 3'-polyU tail (UUUU-3'-OH). The resultant
83 map yielded an overall 3.8 Å resolution telomerase holoenzyme with 4-5 Å local resolution for p65-
84 TER (Figure 1C and Figure S1B-D), improved from ~6 Å.³⁴ The reconstruction shows well-resolved
85 density for almost all of p65 starting from residue 83 in the NTD and of the interacting TER S1-SL4
86 and PK (Figure 1D, Figure S1). S1-SL4 including the single-strand regions were *de novo* modeled
87 assisted by NMR data on TER constructs. The crystal structure of xRRM2²⁵ fit the density with minor
88 refinement. The previously reported homology model of LaM and its interface with S1, PK and the 3'-
89 polyU tail³⁴ was improved by manual fitting and Rosetta refinement. p65 RRM1, whose structure had
90 not been previously determined, was initially built using a homology model to human genuine La
91 protein RRM1³⁴. An additional helix following RRM1 was identified in the density and assigned as
92 RRM1 α 3 (Figure 1D). Two more protein helices were identified in the density and, based on our NMR
93 and other studies discussed below, assigned to the NTD (α N) and the linker region between RRM1
94 α 3 and xRRM2 (α L) (Figure 1D). Combining cryo-EM and NMR studies we also obtained a better
95 model of p65-bound TER, including the 5' and 3' ends, S1, SL4, PK, and single-stranded regions
96 linking PK to S1 and S1 to SL4.

97 p65 interacts along almost the entire S1-SL4 and additionally contacts the PK together forming a
98 U-shape attached to the TERT ring (Figure 1D). The LaM and xRRM2 are at the left and right of the
99 "U" separated by ~64 Å. In addition to the La module binding the 3'-polyU tail, LaM interacts with the
100 ends of S1 and stem 4 (S4) and with the PK, and xRRM2 interacts with central S4 and the GA bulge
101 (Figure 1B and D). Binding of p65 fixes the relative positions of S1-SL4. All three newly identified p65
102 helices— α N, RRM1 α 3, and α L—contribute to RNA recognition and/or p65 domain stability, as
103 discussed in detail below.

104 **La module RRM1 has a C-terminal helix α 3 required for stable folding**

105 RRM1 is positioned on the outer edge of telomerase near the bottom of the U. In the cryo-EM density
106 map the local resolution of RRM1 (~5 Å) is lower than that of LaM (~4 Å) (Figure S1D), suggesting
107 RRM1 is positionally dynamic. Consequently, we were only able to build a homology model of this
108 highly conserved domain refined with Rosetta. The La module RRM1 has the typical β - α - β - β - α - β fold
109 with anti-parallel β -strands stacked on the two α -helices and conserved RNP1 sequence on β 3 and
110 RNP2 sequence on β 1,¹ plus additional N-terminal α 0 and C-terminal α 3 helices (Figure 2A). In the

111 Rosetta model, the long (~18 residues) helix α 3 following RRM1 β 4 appears to be positioned on the β -
112 sheet at its N-terminal end by a stacking interaction between W336 from α 3 and Y250 from RRM1 β 1
113 (Figure 2B). Y250 is part of RNP2 that typically binds RNA, but here mediates the interaction with β 3.
114 Sequence alignment suggests a similar stacking between α 3 and β 1 residues could form in all other
115 identified LARP7 proteins (Figure 2C). Consistent with this, the crystal structure of RRM1 in human
116 genuine La protein La module shows stacking between β 1 Y114 and a helix α 3 Y188,⁴ and the recent
117 cryo-EM structure of human Larp7 in core 7SK RNP has a stacking interaction between RRM1 β 1
118 Y128 and α 3 W384.³⁵ (A previous crystal structure of human Larp7 La module was missing β 4 and
119 α 3.²⁷) Beyond the stacking interactions there is a small kink in the helix and the remainder of the helix
120 protrudes out from the β -sheet of RRM1. This part of α 3 parallels the backbone of proximal S4, but
121 seems to have no direct interactions (Figure 1D).

122 Previous attempts to express or purify p65 La module or RRM1 alone failed, likely due to lack of
123 knowledge on the domain boundaries.^{25,26,30} Based on the cryo-EM model, we designed p65 La
124 module (LaMod(108-355)) and RRM1 (RRM1(240-355)) constructs that include the newly identified
125 α 3 to test the importance of this helix for RRM1 folding and stability, and found that the protein
126 domains could be expressed and purified. RRM1 constructs that include the entire α 3 (RRM1(240-
127 355)) or the first three turns of helix α 3 (RRM1(240-342)) give ^1H - ^{15}N heteronuclear single quantum
128 coherence spectroscopy (HSQC) NMR spectra that indicate RRM1 is folded (Figure 2D,E). In
129 contrast, ^1H - ^{15}N HSQC spectra of RRM1(240-339) shows line broadening or disappearance of the
130 majority of peaks, as well as sample precipitation over time, indicating that it is not stably folded
131 (Figure 2F). Although this shorter construct potentially includes 2 turns of helix α 3, it is apparently not
132 long enough to form a stable interaction between W336 and Y250. Similar results were obtained for
133 α N-LaMod(67-355) versus α N-LaMod(67-335) (Figure S2). To confirm the importance of the stacking
134 interaction between α 3 W336 and β 4 Y250 for stable RRM1 folding, we made a W336A substitution in
135 the context of RRM1(240-355). ^1H - ^{15}N HSQC spectra of this construct show decrease in intensity and
136 chemical shift changes of many peaks, as well as sample precipitation over time, indicating significant
137 destabilization of the domain (Figure 2G). Together, the cryo-EM model, sequence conservation of
138 these residues, observation of similar stacking interactions in other LARP7 proteins, and the NMR

139 data indicate that α 3 is part of RRM1 and is required for a stable fold. More generally, it shows that α 3
140 is a conserved element of LARP7 La modules.

141 **The intrinsically disordered NTD contains a helix α N that binds the La module**

142 The La module was originally characterized for binding the 3'-UUU end of RNA Pol III transcripts and
143 functioning to protect them from degradation.³ It consists of LaM and RRM1 domains connected by a
144 linker that is typically unstructured in the absence of RNA.^{1,3} LaM is a winged-helix motif with an
145 alpha-beta fold comprising a 3-stranded β -sheet and 6 α -helices (Figure 3).^{1,36} p65 LaM has a non-
146 conserved 23 residue loop between LaM α 4 and α 5, and α 5 is unusually long (Figure S3). Deletion of
147 the LaM α 4- α 5 Loop (Δ 174-197), which is not visible in the cryoEM map, does not affect the overall
148 fold of La module, as determined by ^1H - ^{15}N HSQC spectra (Figure S2). After refining the previously
149 reported p65 LaM structure³⁴ and modeling RRM1 into the cryo-EM map, there was still unassigned
150 albeit relatively weak density between LaM and RRM1 that could be fit with an ~18 residue helix
151 (Figure 3A and B).

152 Since all residues in the La module had been assigned to sequence during modeling, we
153 investigated whether this helix came from the NTD. NTD was predicted by Jpred³⁷ to be an
154 intrinsically disordered protein region (IDR). We expressed and purified NTD (residues 1-109), and
155 determined its backbone ^1H , ^{15}N , and ^{13}C assignments by heteronuclear NMR spectroscopy (Figure
156 3C and Figure S4). NMR ^1H - ^{15}N HSQC (Figure 3C) and circular dichroism (CD) spectra (Figure S4C)
157 confirm that NTD is indeed an IDR. Secondary structure propensity (SSP) predictions derived from
158 NMR backbone chemical shifts³⁸ also indicate that most of the NTD is unstructured, but the C-
159 terminus shows moderate interspaced helical propensity (Figure 3D). In the presence of 25 mM SDS,
160 the helical propensity is significantly increased consistent with formation of a continuous helix for
161 residues 87-104, which matches the size of the unassigned helical density in the cryo-EM map
162 (Figure 3A and D). No other distinct density from the NTD was evident in the cryo-EM map. Based on
163 the cryo-EM density map and the NMR data, we conclude that the NTD contains a C-terminal helix
164 that interacts with the La module in the telomerase p65-TER structure.

165 We investigated whether NTD interacts with the La module in the absence of TER or telomerase
166 in solution by NMR spectroscopy. Titration of NTD (residues 1-109) with the La Module (residues 108-
167 355) showed that the two domains interact and the binding is in slow exchange on the NMR time

168 scale, as assayed by ^1H - ^{15}N HSQC (Figure 3C and Figure S4D). The resonances that are affected the
169 most are from αN residues. We then investigated the interactions of αN , LaM, and RRM1 by
170 comparison of ^1H - ^{15}N HSQC spectra of LaM, RRM1, La Module (LaMod(108-355)), and αN -La
171 Module (αN -LaMod(67-355)). Individual spectra of LaM and RRM1 overlay well with LaMod(108-355),
172 indicating that LaM and RRM1 fold as independent domains connected by a flexible linker, as
173 observed for genuine La and human Larp7 (Figure 3E).^{4,39} However, when αN is included (αN -
174 LaMod(67-355)), there are significant chemical shift and linewidth changes in the spectrum consistent
175 with αN interacting with LaM and RRM1 and the domains no longer tumble independently (Figure 3F).
176 We conclude that αN binds the La module in the absence of RNA as well as in the context of
177 telomerase.

178 **The αN -La module interacts with four uridines at the 3'-end**

179 In the cryo-EM structure, NTD αN inserts between LaM and RRM1 (Figure 4A). αN has apparent
180 interactions with LaM α 1, α 5- β 2 loop, and linker following β 3 on one helical face, and with RRM1 α 1,
181 β 2 and β 3- α 2 loop on the opposite face. The insertion of αN results in the RRM1 and LaM being
182 wedged apart by 50° (Figure 4B). Previous NMR studies of human genuine La protein indicated that
183 upon binding with UUU-3'-OH the LaM and RRM1 domains form hydrogen-bonding interactions (Y23-
184 N139 and R57-D125) and tumble as a single domain.⁴⁰ Similar to genuine La, human Larp7 also has
185 individually tumbling LaM and RRM1 in the free La module, and the two domains form a hydrogen-
186 bonding interaction (K53-E172) upon RNA binding. In contrast, p65 LaM and RRM1 bound to TER in
187 the telomerase RNP are in a more open conformation that precludes the formation of the interdomain
188 hydrogen bonds between the equivalent residues on LaM and RRM1 (Figure 4A). The four Us found
189 at the TER 3'-end all interact with the αN -La module (Figure 4C). In the crystal structure of human
190 genuine La with polyU⁴ and cryo-EM structure of Larp7 with 7SK RNA,³⁵ three terminal nucleotides
191 (UUU) bind in a conserved binding pocket between LaM and RRM1 in a V-shape, having alternating
192 interactions with LaM and RRM1 (Figure 4D). A similar V-shaped arrangement is observed in p65,
193 with the first and third U from the 3'-end stacking and binding the LaM (Figure 4C). However, instead
194 of the penultimate U binding to RRM1, which is too far away due to αN wedging LaM and RRM1
195 apart, it interacts with the N-terminal end of αN (Figure 4C). The fourth-to-last nucleotide (U156)
196 interacts with RRM1, where it appears to contact K281 in the β 2- β 3 loop (as judged by their merged

197 densities in the cryoEM map (Figure 4C). Gel shift experiments show that LaMod(108-355) binds to
198 TER construct S1hp-S4hp, that includes the 3'-UUUU-OH, 1.2 fold more weakly than α N-La module
199 (α N-LaMod(67-355)) (Table 1 and Figure 4E). Based on the cryo-EM, EMSA, and NMR data we
200 conclude that α N-La module interacts with the last four nucleotides in the 3'-polyU tail, which bind
201 alternately RRM1-LaM- α N-LaM.

202 The C-terminus of α N also contacts the PK in the minor groove near U92 (Figure 3A), although
203 the density in this region is too weak to assign specific protein side-chain interactions. The α N
204 contacts with U158 in the polyU tail and with the PK explain previous biochemistry results that
205 deletion of NTD decreases p65 binding affinity with TER by two-fold and increases the susceptibility
206 of S1 to RNase One.³⁰ In summary, the NTD α N functions to stabilize a more open form of the La
207 module (compared to La protein and Larp7) and plays a role in both polyU and PK interactions.

208 **LaM binding remodels the PK and fixes the positions of multiple regions of TER**

209 The improved map and resulting model of LaM provide new details about its interaction with other
210 regions of TER besides the 3'-UUUU-OH (Figure 5).³⁴ LaM inserts at a V-shaped junction between
211 PK-S1-CAA-S4, fixing their positions relative to each other. The PK forms one side of the V while S1-
212 CAA-S4 proximal end stack on each other to form the other side of the V (Figure 5A-C). Binding of
213 LaM induces a conformational rearrangement of the PK relative to that observed for the free PK by
214 NMR.⁴¹ In the absence of p65, the free PK has a C75•G95_{syn}-A80 base triple and a U74•A94-U81
215 base triple formed between Stem B and Loop A (Figure 5G). In complex with LaM, A80 forms a non-
216 Watson-Crick base pair with G95, while C75 flips out and inserts into a positively charged channel
217 formed by LaM β 2 and β 3 (K221, K223, K228, K230, R232), which also interact with the backbone of
218 neighboring nucleotides (U74 and A76) (Figure 5A,D,E,H). In addition, K150 from β 1 contacts the
219 backbone of C75 (Figure 5B,D). The PK junction region is also rearranged. Although the stem-stem
220 stacking remains the same, U73 from Loop A swaps with U92 from Stem B and forms a new base
221 pair U73-A83 in Stem A and U92 flips out in Loop B (Figure 5H). This rearrangement shortens Loop
222 A to 2 nucleotides that span the 7-base pair Stem B along the major groove, and results in a more
223 compact PK structure. The unexpected interaction between PK and p65 LaM provides a structural
224 basis for why and how p65 rescues the misfolding of PK caused by mutations.^{41,42}

225 LaM also interacts with S1 to lock S1 in a fixed position relative to PK. Positively charged residues
226 from LaM α 3 (K156, K160) and α 5 (K203) interact with the end of S1 on the major groove side (Figure
227 5A and B), however, individual nucleotides of S1 near the 5'-end could not be unambiguously
228 assigned to the density. Therefore, to determine the positions of nucleotides at the end of S1,
229 including the predicted single stranded 5'-AUA₁₋₃ and 3' ACAA₁₀₈₋₁₁₁, we synthesized S1 hairpin
230 constructs that contain the 5'-end AUA₁₋₃ with or without ACAA₁₀₈₋₁₁₁ linker to SL4 (S1hp and S1hp-
231 ACAA, respectively). The NMR data indicate that in free S1hp-ACAA, U₂ is unexpectedly base paired
232 with A₁₀₈ (Figure S5), extending S1 5'-end by one base pair and decreasing the single-strand S1-S4
233 linker from 4 to 3 nts (CAA). The U₂-A₁₀₈ base pair can be modeled into the cryo-EM density map,
234 with the terminal A₁ base flipped out to stack on the PK and LaM α 2 stacking on the terminal U₂-A₁₀₈
235 base pair (Figure 5F). The relative orientation of S1 and SL4 is fixed by the interaction between LaM
236 and S1-SL4 linker CAA₁₀₉₋₁₁₁. Thus, LaM interacts with both the 5' and 3' ends of TER, where it could
237 function to stabilize the terminal base pairs in S1 and protect both ends from nucleolytic degradation.
238 The 5'-end AUA₁₋₃ and S1-SL4 ACAA₁₀₈₋₁₁₁ linker are highly conserved among *Tetrahymena* species
239 so that similar ends could form,⁴³ while other identified ciliate TERs (*Paramecium*, *Euplotes*,
240 *Oxytricha*, and *Stylonychia* families) lack the 5' single-stranded residues altogether.

241 In contrast to the numerous interactions that fix LaM on TER, RRM1 has only limited interactions
242 with TER, contacting a single U in the polyU tail. RRM1 α 3 parallels proximal S4 but seems to have
243 no direct or fixed interactions (Figure 1D). This is consistent with the higher conformational
244 heterogeneity of RRM1 observed during cryo-EM data processing (Figure S1A) and the lower
245 resolution of RRM1 in the final cryo-EM reconstruction (Figure S1D) compared to LaM. The structure
246 determined here illustrates that LaM serves multiple roles in remodeling and orienting regions of TER,
247 including linking the 5' and 3' ends. La family proteins are known as RNA chaperones in addition to
248 binding the polyU tail to protect the RNA from degradation, but the structural basis of their chaperone
249 function has remained largely unknown. Here we see that for p65 not only the xRRM2 but also the
250 LaM play specific roles in TER folding.

251 **A helix α L stabilizes the interaction of xRRM2 to S4**

252 The xRRM2 was proposed as the recognition domain of p65 specific for *Tetrahymena* TER.⁴⁴ The
253 xRRM2 structure consists of an atypical RRM β - α - β - β - α - β' - β - α fold, where α 3 lies across the surface

254 of the β -sheet where single-stranded RNA nucleotides usually bind in canonical RRM₁s, and it lacks
255 the canonical RNA-binding RNP1 and RNP2 sequences, but contains an RNP3 sequence that can
256 recognize single-stranded RNA nucleotides.^{19,44} Previous biochemical and structural studies have
257 shown that p65 xRRM₂ induces a conformational change in S4 via interactions with the conserved
258 GA bulge and adjacent base pairs.^{23,25,26,42} This conformational change bends S4 by \sim 60°, thereby
259 helping position loop 4 for interaction with TERT, where it inserts between TERT RNA binding domain
260 (TRBD) and C-terminal element (CTE), thereby stabilizing the TERT ring. As observed in the xRRM₂–
261 S4 crystal structure,²⁵ xRRM₂ α 3 inserts from the major groove side between the base pairs on either
262 side of the GA bulge, to bend S4, and the GA bulge residues flip out to interact in a binding pocket
263 between β 4 (RNP3) and helix α 3. In the context of full-length S4 in telomerase, we find that p65 has
264 additional interactions to S4 from xRRM₂ α 1 and the RRM₁-xRRM₂ linker, that were not present in
265 the xRRM₂ structure co-crystallized with central S4 and the GA bulge (Figure 6A and B). K392 from
266 helix α 1 of p65 xRRM₂ contacts the minor groove of distal S4, interacting with the backbone of C142
267 in S4 (Figure 6C). The S4 construct in the crystal structure had a distal stem of 4 base pairs and did
268 not include the C₁₄₂-G₁₂₈ base pair.²⁵ Sequence alignment of LARP7s and human La protein shows
269 that the equivalent K392 position is always a positively charged residue (Figure S6). The equivalent
270 residue from human Larp7 xRRM₂ α 1 (R468) forms a hydrogen bond with 2'OH of the RNA.²⁸

271 A C-terminal helix α 3 in RRM₁ and a linker between RRM₁ α 3 and xRRM₂ are present in all
272 identified LARP7 proteins (Figure S6). The cryo-EM density assigned to the linker indicates that it is a
273 helix, here named α L. Helix α L and xRRM₂ α 3 are positioned almost antiparallel to each other in the
274 complex. The density for helix α L, that was not part of the xRRM₂ construct used in the crystal
275 structure²⁵ is relatively weak compared to helix α 3, so sidechain interactions cannot be discerned.
276 Based on the model, α L and α 3 interact, most likely via charge interactions as well as a hydrophobic
277 interaction at each end. Helix α L also appears to contact S4, most likely via the positively charged
278 residue R362 to the RNA backbone near U117. While the non-conserved bulge U117 appears flipped
279 out to potentially contact α L, deletion of this residue has no effect on xRRM–SL4 binding (Table 1 and
280 Figure S7) or on activity.⁴⁵

281 Although α L appears to be part of xRRM₂ in the complex (Figure 6), p65 xRRM₂ as well as
282 xRRM₂ from other LARP7 proteins folds as a standalone functional domain without the N-terminal

283 helix α L, based on structures determined to date.^{19,20,25,29} NMR ^1H - ^{15}N HSQC spectra show that p65
284 xRRM2 domain folds the same with or without helix α L and that helix α L has a minor effect on the
285 chemical shifts of residues from xRRM2, mainly affecting residues 376-379 preceding β 1 (Figure S8).
286 TALOS-N scores calculated from backbone chemical shift assignments showed that the α L residues
287 do not form a helix in the absence of RNA; however, additional resonances from α 3x residues (aa
288 527-539) were observed in α L-xRRM2 that were not present in xRRM2 alone and TALOS-N scores
289 indicate helical conformation for residue 527 (Figure S8C). These α 3x residues were previously
290 indicated to be dynamic in xRRM2 and only form a helix upon binding S4.²⁵ Thus, these NMR
291 observations indicate that α L residues do transiently interact with α 3x residues in the absence of RNA
292 to promote the stability of α 3x, but both α L and α 3x only fold stably upon binding RNA. This is
293 consistent with binding studies using gel shifts, where xRRM2 binds to SL4 about \sim 1.6-fold weaker
294 than α L-xRRM2 does (Figure 6D, E, and Table 1). Therefore, α L interaction with α 3 stabilizes the
295 interaction of xRRM2 with S4, likely through stabilization of α 3x folding and enhanced interactions
296 with SL4. Thus, these results suggest that the α L cooperates with xRRM2 to tightly bind and orient
297 SL4 at a precise angle to dock loop 4 into the TRBD-CTE interface.

298 **DISCUSSION**

299 Previous studies of genuine La and LARP7 proteins have shown that the La module binds and
300 protects the 3'-poly U ends of RNA polymerase III transcripts⁴⁶ while a C-terminal xRRM2, separated
301 by a linker of variable length, determines specificity for specific (or non-specific for genuine La) RNA
302 substrates.^{1,47} Earlier studies established that p65 xRRM binds and bends SL4 to position loop 4 for
303 interaction with TERT at the interface between TRBD and CTE. However, it has been unclear how
304 p65-TER interactions can collectively orient the SL4 at the correct location during assembly, because
305 the free TER has several intrinsically flexible regions (i.e., single-stranded linkers and bulges)
306 between and within the rigid structural units (i.e., S1, SL4, and PK), and the free p65 has domains (La
307 motif, RRM1, xRRM2) connected by flexible linkers. Here, using a combination of cryo-EM, NMR
308 spectroscopy and Rosetta modeling, we determined the structure of *Tetrahymena* telomerase LARP7
309 protein p65 bound to TER in the context of its native RNP telomerase. We find that virtually the entire
310 'linker' between the canonical end of RRM1 and the start of xRRM2 forms helices—RRM1 α 3 and
311 α L—contribute with the La module and xRRM2 in orienting TER for interaction with TERT, and that

312 the intrinsically disordered NTD contains an incipient helix that orders LaM and RRM1 in the La
313 module.

314 The hybrid approach used here should be generally applicable to other complex biological
315 systems where flexibility, conformational dynamics, or structural heterogeneity limit the overall
316 resolution of cryoEM maps. In this study, NMR was used to characterize the intrinsically disordered
317 NTD and identify NTD helix α N; show that RRM1 helix α 3, in particular stacking interactions between
318 α 3 W336 and β 1 Y250, is required for domain stability; show that α N binds LaM and RRM1 in the
319 absence of TER in solution as well as with TER in telomerase; show that α L and xRRM2 α 3x only fold
320 stably when xRRM2 binds TER; and identify RNA base pairs at the 5' and 3' ends of TER. These
321 results not only made it possible to model the p65–TER complex in the cryoEM density map, but also
322 provided insights into assembly of p65 with TER.

323 Telomerase activity requires two conserved domains of TER, t/PK that is closed by a helix, stem 1
324 in *Tetrahymena*, and STE, stem-loop 4 in *Tetrahymena*, that binds the TRBD and CTE interface to
325 help close the TERT ring. The structure of p65–TER reveals that p65 links these two elements,
326 binding the PK, stem 1 that includes the 5'-end, the polyU tail at the 3'-end of stem 4, and stem 4. A
327 helix α N in the otherwise unstructured NTD cooperates with the La module to bind the 4 Us at the 3'-
328 end of TER in a binding pocket similar to but divergent from genuine La protein. While RRM1 has only
329 one apparent contact with TER, with the U four nts from the 3'-end, the LaM interacts not only with the
330 polyU tail, but, as previously observed at lower resolution,³⁴ also with S1, proximal S4, PK, and the 5'-
331 end. These contacts are buttressed by the unanticipated interaction of an NTD helix α N with the La
332 module, with direct contacts from α N to both the PK and the penultimate U. Together, the interactions
333 of p65 along the entire length of the RNA from PK to S1 to S4 reveal how it can precisely position
334 loop 4 for interaction with the TERT ring. These interactions also link the positions of the PK and the
335 STE, two essential elements of TER for activity.

336 The p65 RRM1 helix α 3 appears to be common to genuine La and LARP7 RRM1s, as indicated
337 by the sequence alignment (Figure S3). A helix α 3 is present in the crystal structure of human
338 genuine La protein in complex with UUU⁴ and in the cryo-EM structure of human Larp7 in complex
339 with its 7SK RNA substrate. In contrast, helix α N may be unique to *Tetrahymena* p65, where it helps
340 determine protein specificity for telomerase RNA. Helix α N wedges between the LaM and RRM1,

341 while in genuine La protein and human Larp7 these two domains directly interact via hydrogen bond
342 interactions when bound to polyU. Intriguingly, in yeast telomerase, Pof8, a homologue of
343 *Tetrahymena* p65, has also recently been shown to interact with both PK and UUU-3'-OH, but the
344 latter interaction is via Lsm2-8.²⁰

345 To date, there are only two structures of a full-length La related protein bound to RNA, p65
346 reported here and hLarp7 that is a core component of 7SK RNP.³⁵ Both proteins utilize linker helices
347 and extensions to augment specific interactions from their globular LaM, RRM1, and RRM2 domains,
348 but in significantly different ways. In p65, NTD helix α N wedges the two domains of La module apart
349 and helps to stabilize the pseudoknot of TER and linker helix α L stabilizes RRM2 α 3x residues to
350 assist in S4 interactions. In hLarp7, a C-terminal helix α 4 following xRRM2 interacts with RRM1 helix
351 α 3, via 7SK RNA SL4 anchoring for both helices. These two helices form the protein-protein interface
352 with MePCE, the other 7SK core RNP protein component. In addition, Larp7 RRM1 interacts with six
353 out of eight polyU tail (UUUCUUUU) nucleotides vs one in p65. The two structures illustrate a general
354 concept that protein and RNA regions that are flexible linkers in the free subunits often become
355 ordered in the protein–RNA complex, highlighting their importance for highly specialized complex
356 formation and RNA specificity.

357 The p65–TER interactions provide new insights into assembly of TER with TERT (Figure 7). In
358 *Tetrahymena*, telomerase RNP assembly begins with binding of chaperone protein p65 to TER,²²
359 where it may displace *Tetrahymena* genuine La protein. Previous studies have suggested that the
360 free TER favors a lower energy Stem 3 alternative conformation (S3alt) over the PK, generating a
361 small circle linked to SL4 through a short single-stranded linker (Figure 7A).⁴¹ In the first step, the p65
362 La module interacts with both ends of TER to fix the S1-S4 angle and protect the TER ends from
363 nucleolytic degradation, and p65 xRRM2 together with α L specifically recognizes the S4 GA bulge
364 and bends SL4 (Figure 7B). In one possible scenario for the second step, the t/PK circle is opened
365 through the unfolding of S3alt by TERT binding and/or an endogenous helicase, so that the TERT ring
366 can enter the t/PK circle prior to pseudoknot formation. Nucleotides adjacent to S2 are anchored on
367 TERT TRBD and the template interacts with the RT domain, and the TERT ring closure is stabilized
368 by p65-oriented SL4 inserting between CTE and TRBD.³¹⁻³³ Finally, p65 interactions stabilize the
369 pseudoknot fold and help to lock it onto the TERT ring (Figure 7C). In summary, using an integrative

370 structural biology approach we solved the structure of full-length p65 in complex with TER in
371 telomerase, which provides insights into its roles as an RNA chaperone and integral component of
372 telomerase RNP and sheds light on similar functions for other La and LARP family proteins.

373 **MATERIALS AND METHODS**

374 **Telomerase sample preparation**

375 *Tetrahymena* telomerase was purified following the previously described protocol,³³ with minor
376 modifications. Sixteen liters of *Tetrahymena* TERT-FZZ cells were grown in PPYS media. The cells
377 were harvested by centrifugation, washed with 20 mM HEPES·NaOH pH 8.0, and then lysed in lysis
378 buffer (20 mM HEPES·NaOH pH 8.0, 50 mM NaCl, 1 mM Ethylenediaminetetraacetic acid (EDTA), 1
379 mM tris(2-carboxyethyl)phosphine (TCEP), 10% glycerol, 0.2% IGEPAL CA-630, 0.1% Triton X-100)
380 at 4 °C for 30 min. After ultracentrifugation at 230,000 × g for 1 hour, the supernatant of the cell lysate
381 was incubated with Rabbit-IgG agarose slurry (Sigma) overnight at 4 °C. The resin was washed with
382 wash buffer (20 mM HEPES·NaOH pH 8.0, 50 mM NaCl, 1 mM MgCl₂, 1 mM TCEP, 10% glycerol,
383 0.1% IGEPAL CA-630). TEV protease was added into the solution to elute telomerase from IgG resin.
384 During this step, 5 µM single-stranded telomeric DNA (sstDNA) was added to saturate telomerase.
385 The elution fraction was incubated with anti-Flag M2 affinity gel (Sigma) for 1 hour at 4 °C. After that,
386 the anti-Flag resin was washed extensively with wash buffer and eluted using glycerol-free buffer (20
387 mM HEPES·NaOH pH 8.0, 50 mM NaCl, 1 mM MgCl₂, 1 mM TCEP, 0.1% IGEPAL CA-630)
388 supplemented with 1 mg/mL 3× FLAG peptide.

389 **Cryo-EM specimen preparation and data collection**

390 Lacey carbon grids with a supporting ultrathin carbon film (Ted Pella) were used for cryo-EM sample
391 preparation. 3 µL of sample was applied to glow-discharged grid, then blotted with filter paper and
392 flash-frozen in liquid ethane using an FEI Vitrobot Mark IV. Vitrified cryo-EM grids were loaded into an
393 FEI Titan Krios electron microscope at 300 kV for automated image acquisition with SerialEM.⁴⁸
394 Movies of dose-fractionated frames were acquired with a Gatan K2 Summit direct electron detector
395 operated in super-resolution mode, yielding a pixel size of 0.68 Å on the sample level. A Gatan
396 Imaging Filter (GIF) was installed between the electron microscope and the K2 camera with the slit
397 width setting to 20 eV. The dose rate on the detector was set to ~ 6 electrons/Å²/s and the total
398 exposure time of each movie was 8 s, which fractionated into 40 frames of images with 0.2 s

399 exposure time for each frame. In total, 12,922 movies for telomerase bound with
400 (GTTGGG)₂GTTGGG^LG^LT^LT sstDNA (dataset1, T^L/G^L represents locked nucleic acid oligonucleotide),
401 and 13,097 movies for telomerase bound with (GTTGGG)₅ sstDNA (dataset2) were collected in
402 separate imaging sessions.

403 **Cryo-EM data processing**

404 Dose-fractionated frames except for the first of each movie were 2 \times binned (pixel size of 1.36 Å) and
405 aligned for correction of beam-induced drift using MotionCor2.⁴⁹ The contrast transfer function (CTF)
406 parameters were determined by CTFFIND4.⁵⁰ All micrographs after motion correction and their power
407 spectra were visually inspected, and the micrographs with too much thick carbon area, ice
408 contamination or defocus value outside the range from -0.8 to -4.0 μm were discarded. Gautomatch
409 was used for particle picking with template projections obtained from a previous reconstruction (EMD-
410 7821).³¹

411 The cryo-EM data processing procedure is outlined in Figure S1A. Two datasets were initially
412 processed separately in two batches using RELION 3.0.⁵¹ For dataset1, 3,951,762 particles were
413 initially picked and screened as previously described.³⁴ The resulted 924,041 particles were refined
414 with a soft mask (mask1) to obtain orientation parameters of each particle, which were used as inputs
415 for the following 3D classification with local angular search (RELION options: --sigma_ang 12).
416 487,859 particles in two good classes were combined and subjected to another round of 3D
417 classification (RELION options: --skip_align --tau2_fudge 10) with a mask (mask2) encompassing p65
418 La module. 193,669 particles with strong density of p65 La module were eventually selected from
419 dataset1 for the subsequent processing. Dataset2 was processed separately in a similar way, and
420 106,811 particles were selected.

421 Since sstDNA and p65 bind to separate regions of TER without any crosstalk, selected particles
422 from two datasets were combined together to improve the overall resolution of p65. Refinement of the
423 combined 300,480 particles generated an overall 3.5 Å resolution reconstruction. Notably, this
424 resolution was obtained mainly based on high-resolution features of TERT, and the local resolution of
425 p65 was only around 4-5 Å. We have also tried signal subtraction and focused refinement of p65
426 region (p65 together with TER PK, S1 and SL4) alone, but the result was worse than 3D refinement of
427 the whole complex with mask1, probably because the p65 region is too small (stable volume ~70 kDa)
428 to generate enough signal for 3D alignment. Alternatively, we extracted signals of p65 LaM from each

429 particle with mask3 and performed focused 3D classification without alignment (RELION options: --
430 skip_align --tau2_fudge 10). 162,358 particles were selected, followed by CTF refinement and
431 Bayesian polishing. The resulting “shiny” particles were refined with mask1, resulting in a final 3.8 Å
432 resolution reconstruction with improved densities of p65 LaM.

433 Resolutions of the cryo-EM maps were estimated on the basis of the “gold-standard” Fourier Shell
434 Correlation (FSC) = 0.143 criterion.⁵² The cryo-EM maps were corrected for the modulation transfer
435 function (MTF) of the detector, sharpened with a negative B-factor and low-pass filtered to the stated
436 resolution using the *relion_postprocess* program in RELION.⁵¹ Local resolution evaluations were
437 determined by ResMap⁵³ with two independently refined half-maps. Data collection and processing
438 statistics are given in Table S1.

439 **Model building and refinement**

440 The atomic coordinates of p65 and TER were built and refined using Coot⁵⁴ and UCSF Chimera⁵⁵. For
441 the xRRM2 domain (residues 377-417, 453-542), modeling was initiated by fitting of the crystal
442 structure of p65 xRRM2-SL4 (PDB: 4ERD) into the cryo-EM map, and further manually adjusted in
443 Coot. A homology model of La module was initially generated by the SWISS-MODEL server using the
444 crystal structure of human La protein (PDB: 2VOO) as template. The generated LaM model (residues
445 112-231) shows there is flexible p65-specific loop between α4 and α5 (residues 174-197), which was
446 deleted during the subsequent modeling. LaM alone was unambiguously fitted into the cryo-EM
447 density in Chimera. The orientation and location of RRM1 model (residues 240-331) was manually
448 fitted into the density using the conserved interfaces among RRM1, LaM, and UUU-3'-OH of human
449 La protein. For NTD, the secondary structure information was obtained from NMR chemical shift, the
450 C-terminus (residues 87-104) was modeled as an ideal helix. These generated individual models
451 were served as starting coordinates for rebuilding the p65 (residues 83-542) in RosettaCM⁵⁶. 3000
452 models were calculated, and the top scoring hits were manually inspected in Coot.

453 The initial TER model was adopted from previous model (PDB: 6D6V). The residues in PK and
454 SL4 parts with high resolution cryo-EM features were manually adjusted for their base conformation
455 against the density map. The secondary structure of S1 was obtained from NMR data, and then was
456 manually fitted into the density map. The UUU157-159 were initially adopted from the crystal structure
457 of human La protein with UUU-3'-OH (PDB: 2VOO), and then were manually adjusted against the

458 density. The remaining linker and single-stranded regions connecting the secondary structure
459 elements discussed above were modeled into the density map using Coot.

460 The entire p65-TER complex was refined in Phenix⁵⁷ using “phenix.real_space_refine” with
461 secondary structure, Ramachandran, and rotamer restraints, and was further refined by ISOLDE in
462 ChimeraX⁵⁸. Structural models were validated using Molprobity⁵⁹.

463 **p65 expression and purification**

464 The DNA encoding NTD, LaM, RRM1, La module, α N-La module and α L-xRRM2 constructs were
465 cloned into pETDuet vector, which was further modified to include a hexahistidine (His₆) tag followed
466 by a tobacco etch virus (TEV) protease cleavage site at the N terminus before the protein sequence.
467 For α L-xRRM2, a β 2- β 3 loop truncation was included as described previously.²⁵ Protein point
468 substitutions/deletions were carried out with a Q5 site-directed mutagenesis kit (NEB) and verified by
469 DNA sequencing. All the constructs were transformed into *Escherichia coli* BL21-Gold (DE3) for
470 protein expression. Bacterial cultures were grown in M9 minimal medium at 37 °C to an OD₆₀₀ of 0.6-
471 0.8, then transferred to 18 °C for 1 h before induction with 0.5 mM isopropyl β -d-1-
472 thiogalactopyranoside (IPTG) for 18 h. Cells were harvested by centrifugation and the pellets were
473 resuspended with resuspension buffer (20 mM HEPES, pH 8, 1 M NaCl, 1 mM TCEP, 15 mM
474 imidazole, 5% glycerol, and 1 mM PMSF) supplemented with lysozyme, then sonicated on ice. Cell
475 lysate was clarified by centrifugation and filtration, and the His₆-tagged proteins were purified with a
476 nickel affinity column and further purified on an S75 column attached to an AKTA FPLC (GE
477 Healthcare) using NMR buffer.

478 ***In vitro* transcription and purification of RNA**

479 All TER RNA constructs were prepared by *in vitro* transcription using T7 RNA polymerase (P266L
480 mutant)⁶⁰ with synthetic DNA templates (Integrated DNA Technologies) as described previously.⁶¹
481 After *in vitro* transcription, the RNA samples were ethanol precipitated, purified using 15%-20%
482 denaturing polyacrylamide gels, electroeluted with Elutrap system (Whatman), and further purified by
483 anion exchange with a 5-mL Hi-Trap Q column (GE Healthcare). All purified RNA was desalting and
484 exchanged into nanopure water using an Amicon filtration system with 3,000 molecular weight cutoff
485 membranes (Millipore). RNA samples were diluted to concentrations of ~10 μ M in the desired buffer
486 containing 10 mM potassium phosphate, heated at 95 °C for 3 min, snap-cooled on ice for 30 min,
487 and then concentrated for NMR and gel shift experiments.

488 **NMR sample preparation and data collection**

489 For the assignment of NTD, 0.3 mM sample uniformly enriched with ^{15}N and ^{13}C in 20 mM sodium
490 phosphate, pH 7.0, 50 mM NaCl, and 2 mM DTT, 0.02% NaN₃, 5% v/v D₂O was used. NMR spectra
491 were recorded on Bruker DRX 600 MHz and Avance 800 MHz spectrometers equipped with HCN
492 cryogenic probes at 298 K. The backbone assignment (83% completion) was achieved from analysis
493 of HNCACB, CBCA(CO)NH, HNCA and C(CO)NH spectra. The NMR data of ^{13}C , ^{15}N -labelled α L-
494 xRRM2 with helix α L was collected on Bruker DRX 600 MHz spectrometers in NMR buffer (20 mM
495 sodium phosphate, pH 6.1, 50 mM KCl, 1 mM TCEP, 5% v/v D₂O) at 298 K. The backbone
496 assignment of ^{13}C , ^{15}N -labelled α L-xRRM2 (69% completion) was achieved from analysis of HNCACB,
497 CBCA(CO)NH, HNCA and CC(CO)NH, aided by previous NMR assignments of xRRM2. Spectra of all
498 RNA samples (0.5 mM to 1 mM in 10 mM sodium phosphate, pH 6.4, 50 mM KCl, 10% v/v D₂O) were
499 collected on Avance 800-MHz spectrometer at 283 K. To assign the 1D imino proton spectra,
500 exchangeable-proton NOESY spectra were recorded. All other p65 domain samples were in 20 mM
501 sodium phosphate, pH 7.0, 50 mM KCl, 1 mM TCEP, 10% v/v D₂O and were collected at 298 K on
502 Avance 800-MHz spectrometer. The NTD and LaMod(108-355) binding experiments were conducted
503 by adding LaMod(108-355) to NTD by varying the [NTD]:[LaMod(108-355)] concentration ratio from
504 1:0 to 1:2.0. The protein domains were mixed under diluted conditions and then concentrated using
505 Amicon filtration system (Millipore, 3K MWCO). The final protein concentration of NTD in the NMR
506 samples was 50 μM . NMR spectra were processed and analyzed with Topspin (Bruker), NMRPipe,
507 and NMRFAM-Sparky.

508 **Electrophoretic mobility shift assay (EMSA)**

509 TER (S1hp-S4hp, SL4hp, and SL4hp Δ U117) and p65 (α N-LaMod(67-355), LaMod(108-355), α L-
510 xRRM2 and xRRM2) samples were prepared separately in binding buffer (pH 7.0, 50 mM KCl, and 1
511 mM TCEP). RNA (100 nM for S1hp-S4hp and 150 nM for SL4hp and SL4hp Δ U117, respectively) and
512 protein were mixed at various ratios in a total volume of 10 μl . The complexes were incubated on ice
513 for 1h prior to gel electrophoresis on 5.7% polyacrylamide gel (37.5:1 crosslinking ratio) with 1X TBE
514 buffer at 4 °C. Gels were subsequently stained with SYBR Gold (Invitrogen) and imaged by Pharos
515 FX Plus scanner (Bio-Rad). The signal intensity of the free DNA was quantified with ImageJ software.
516 The binding affinity (K_d) was further determined by fitting the fraction bound values to the following
517 equation

$$\theta = \frac{([Pt] - \frac{[Rt] + [Pt] + K_{Dapp} - \sqrt{([Rt] + [Pt] + K_{Dapp})^2 - 4[Rt][Pt]}}{2})^n}{K_{Dapp}^n + ([Pt] - \frac{[Rt] + [Pt] + K_{Dapp} - \sqrt{([Rt] + [Pt] + K_{Dapp})^2 - 4[Rt][Pt]}}{2})^n}$$

518 where $[Rt]$, $[Pt]$, K_{Dapp} , n and θ are the total RNA concentration, protein concentration, global
 519 dissociation constant, the Hill coefficient, and fraction bound, respectively.

521 **ACCESSION NUMBERS**

522 Cryo-EM density maps and atomic coordinates for p65-focused refinement of *Tetrahymena*
 523 telomerase have been deposited in the Electron Microscopy Data Bank and wwPDB, respectively,
 524 under accession codes EMD- 29903 and PDB 8GAP. Backbone chemical shifts assignments for NTD
 525 (free and SDS-bound) and free α L-xRRM2 and imino assignments for S1hp and S1hp-ACAA have
 526 been deposited in the Biological Magnetic Resonance Data Bank, under accession IDs 51798, 51797,
 527 51808, 51809, respectively.

528 **AUTHOR CONTRIBUTIONS**

529 **Yaqiang Wang**: Conceptualization, Methodology, Formal analysis, Investigation, Data curation,
 530 Writing – original draft, Writing – review & editing, Visualization. **Yao He**: Conceptualization,
 531 Methodology, Formal analysis, Investigation, Data curation, Writing – original draft, Writing – review &
 532 editing, Visualization. **Yanjiao Wang**: Validation, Formal analysis, Investigation, Data curation, Writing
 533 – review & editing, Visualization. **Yuan Yang**: Validation, Formal analysis, Investigation, Data
 534 curation, Writing – review & editing, Visualization. **Mahavir Singh**: Investigation. **Catherine D.**
 535 **Eichhorn**: Data curation, Investigation, Writing – review & editing. **Xinyi Cheng**: Investigation. **Yi**
 536 **Xiao Jiang**: Investigation. **Z. Hong Zhou**: Supervision, Funding acquisition. **Juli Feigon**:
 537 Conceptualization, Data Curation, Writing – original draft, Writing – review & editing, Supervision,
 538 Project Administration, Funding acquisition.

539 **FUNDING**

540 This work was supported by the National Institutes of Health (NIH) R35GM131901 and the National
 541 Science Foundation (NSF) MCB2016540 to J.F, and NIH grant R01GM071940 to Z.H.Z. The NMR
 542 facility was supported in part by NIH instrumentation grants S10OD016336 and S10OD025073 and
 543 Department of Energy DE-FC03-02ER63421. The Electron Imaging Center for Nanomachines was

544 supported by UCLA and by instrumentation grants from NIH [S10RR23057, S10OD018111 and
545 U24GM116792], NSF [DBI-1338135 and DMR-1548924].

546 **Conflict of interest statement.** None declared.

REFERENCES

547 1 Maraia, R.J., Mattijsen, S., Cruz-Gallardo, I., Conte, M.R., (2017). The La and related RNA-
548 binding proteins (LARPs): structures, functions, and evolving perspectives. *Wiley Interdiscip*
549 *Rev RNA*, **8**.

550 2 Wolin, S.L., Cedervall, T., (2002). The La protein. *Annu. Rev. Biochem.*, **71**, 375-403.

551 3 Bayfield, M.A., Yang, R., Maraia, R.J., (2010). Conserved and divergent features of the
552 structure and function of La and La-related proteins (LARPs). *Biochim. Biophys. Acta*, **1799**,
553 365-378.

554 4 Kotik-Kogan, O., Valentine, E.R., Sanfelice, D., Conte, M.R., Curry, S., (2008). Structural
555 analysis reveals conformational plasticity in the recognition of RNA 3' ends by the human La
556 protein. *Structure*, **16**, 852-862.

557 5 Naeeni, A.R., Conte, M.R., Bayfield, M.A., (2012). RNA chaperone activity of human La
558 protein is mediated by variant RNA recognition motif. *J. Biol. Chem.*, **287**, 5472-5482.

559 6 Jacks, A., Babon, J., Kelly, G., Manolaridis, I., Cary, P.D., Curry, S. *et al.*, (2003). Structure of
560 the C-terminal domain of human La protein reveals a novel RNA recognition motif coupled
561 to a helical nuclear retention element. *Structure*, **11**, 833-843.

562 7 Hasler, D., Meister, G., Fischer, U., (2021). Stabilize and connect: the role of LARP7 in nuclear
563 non-coding RNA metabolism. *RNA biology*, **18**, 290-303.

564 8 Markert, A., Grimm, M., Martinez, J., Wiesner, J., Meyerhans, A., Meyuhas, O. *et al.*, (2008).
565 The La-related protein LARP7 is a component of the 7SK ribonucleoprotein and affects
566 transcription of cellular and viral polymerase II genes. *EMBO Rep.*, **9**, 569-575.

567 9 Krueger, B.J., Jeronimo, C., Roy, B.B., Bouchard, A., Barrandon, C., Byers, S.A. *et al.*, (2008).
568 LARP7 is a stable component of the 7SK snRNP while P-TEFb, HEXIM1 and hnRNP A1 are
569 reversibly associated. *Nucleic Acids Res.*, **36**, 2219-2229.

570 10 Muniz, L., Egloff, S., Kiss, T., (2013). RNA elements directing in vivo assembly of the
571 7SK/MePCE/Larp7 transcriptional regulatory snRNP. *Nucleic Acids Res.*, **41**, 4686-4698.

572 11 Wang, Y., Feigon, J., (2017). Structural biology of telomerase and its interaction at telomeres.
573 *Curr. Opin. Struct. Biol.*, **47**, 77-87.

574 12 Chan, H., Wang, Y., Feigon, J., (2017). Progress in Human and Tetrahymena Telomerase
575 Structure Determination. *Annu. Rev. Biophys.*, **46**, 199-225.

576 13 Wang, Y., Susac, L., Feigon, J., (2019). Structural Biology of Telomerase. *Cold Spring Harbor*
577 *perspectives in biology*, **11**.

578 14 Aigner, S., Postberg, J., Lipps, H.J., Cech, T.R., (2003). The Euplotes La motif protein p43 has
579 properties of a telomerase-specific subunit. *Biochemistry*, **42**, 5736-5747.

580 15 Aigner, S., Lingner, J., Goodrich, K.J., Grosshans, C.A., Shevchenko, A., Mann, M. *et al.*,
581 (2000). Euplotes telomerase contains an La motif protein produced by apparent translational
582 frameshifting. *EMBO J.*, **19**, 6230-6239.

583 16 Paez-Moscoso, D.J., Pan, L., Sigauke, R.F., Schroeder, M.R., Tang, W., Baumann, P., (2018).
584 Pof8 is a La-related protein and a constitutive component of telomerase in fission yeast. *Nat*
585 *Commun*, **9**, 587.

586 17 Mennie, A.K., Moser, B.A., Nakamura, T.M., (2018). LARP7-like protein Pof8 regulates
587 telomerase assembly and poly(A)+TERRA expression in fission yeast. *Nat Commun*, **9**, 586.

588 18 Collopy, L.C., Ware, T.L., Goncalves, T., S, I.K., Yang, Q., Amelina, H. *et al.*, (2018). LARP7
589 family proteins have conserved function in telomerase assembly. *Nat Commun*, **9**, 557.

590 19 Basu, R., Eichhorn, C.D., Cheng, R., Peterson, R.D., Feigon, J., (2021). Structure of *S. pombe*
591 telomerase protein Pof8 C-terminal domain is an xRRM conserved among LARP7 proteins.
592 *RNA biology*, **18**, 1181-1192.

593 20 Hu, X., Kim, J.K., Yu, C., Jun, H.I., Liu, J., Sankaran, B. *et al.*, (2020). Quality-Control
594 Mechanism for Telomerase RNA Folding in the Cell. *Cell Rep*, **33**, 108568.

595 21 Witkin, K.L., Collins, K., (2004). Holoenzyme proteins required for the physiological assembly
596 and activity of telomerase. *Genes Dev.*, **18**, 1107-1118.

597 22 Stone, M.D., Mihalusova, M., O'Connor C, M., Prathapam, R., Collins, K., Zhuang, X., (2007).
598 Stepwise protein-mediated RNA folding directs assembly of telomerase ribonucleoprotein.
599 *Nature*, **446**, 458-461.

600 23 Prathapam, R., Witkin, K.L., O'Connor, C.M., Collins, K., (2005). A telomerase holoenzyme
601 protein enhances telomerase RNA assembly with telomerase reverse transcriptase. *Nat.*
602 *Struct. Mol. Biol.*, **12**, 252-257.

603 24 O'Connor, C.M., Lai, C.K., Collins, K., (2005). Two purified domains of telomerase reverse
604 transcriptase reconstitute sequence-specific interactions with RNA. *J. Biol. Chem.*, **280**,
605 17533-17539.

606 25 Singh, M., Wang, Z., Koo, B.K., Patel, A., Cascio, D., Collins, K. *et al.*, (2012). Structural basis
607 for telomerase RNA recognition and RNP assembly by the holoenzyme La family protein p65.
608 *Mol. Cell*, **47**, 16-26.

609 26 O'Connor, C.M., Collins, K., (2006). A novel RNA binding domain in tetrahymena telomerase
610 p65 initiates hierarchical assembly of telomerase holoenzyme. *Mol. Cell. Biol.*, **26**, 2029-
611 2036.

612 27 Uchikawa, E., Natchiar, K.S., Han, X., Proux, F., Roblin, P., Zhang, E. *et al.*, (2015). Structural
613 insight into the mechanism of stabilization of the 7SK small nuclear RNA by LARP7. *Nucleic*
614 *Acids Res.*, **43**, 3373-3388.

615 28 Eichhorn, C.D., Yang, Y., Repeta, L., Feigon, J., (2018). Structural basis for recognition of
616 human 7SK long noncoding RNA by the La-related protein Larp7. *Proc Natl Acad Sci U S A*,
617 **115**, E6457-E6466.

618 29 Eichhorn, C.D., Chug, R., Feigon, J., (2016). hLARP7 C-terminal domain contains an xRRM that
619 binds the 3' hairpin of 7SK RNA. *Nucleic Acids Res.*, **44**, 9977-9989.

620 30 Akiyama, B.M., Loper, J., Najarro, K., Stone, M.D., (2012). The C-terminal domain of
621 Tetrahymena thermophila telomerase holoenzyme protein p65 induces multiple structural
622 changes in telomerase RNA. *RNA*, **18**, 653-660.

623 31 Jiang, J., Wang, Y., Susac, L., Chan, H., Basu, R., Zhou, Z.H. *et al.*, (2018). Structure of
624 Telomerase with Telomeric DNA. *Cell*, **173**, 1179-1190 e1113.

625 32 Jiang, J., Chan, H., Cash, D.D., Miracco, E.J., Ogorzalek Loo, R.R., Upton, H.E. *et al.*, (2015).
626 Structure of Tetrahymena telomerase reveals previously unknown subunits, functions, and
627 interactions. *Science*, **350**, aab4070.

628 33 Jiang, J., Miracco, E.J., Hong, K., Eckert, B., Chan, H., Cash, D.D. *et al.*, (2013). The
629 architecture of Tetrahymena telomerase holoenzyme. *Nature*, **496**, 187-192.

630 34 He, Y., Wang, Y., Liu, B., Helmling, C., Susac, L., Cheng, R. *et al.*, (2021). Structures of
631 telomerase at several steps of telomere repeat synthesis. *Nature*, **593**, 454-459.

632 35 Yang, Y., Liu, S., Egloff, S., Eichhorn, C.D., Hadjian, T., Zhen, J. *et al.*, (2022). Structural basis of
633 RNA conformational switching in the transcriptional regulator 7SK RNP. *Mol. Cell*, **82**, 1724-
634 1736 e1727.

635 36 Dong, G., Chakshusmathi, G., Wolin, S.L., Reinisch, K.M., (2004). Structure of the La motif: a
636 winged helix domain mediates RNA binding via a conserved aromatic patch. *EMBO J.*, **23**,
637 1000-1007.

638 37 Drozdetskiy, A., Cole, C., Procter, J., Barton, G.J., (2015). JPred4: a protein secondary
639 structure prediction server. *Nucleic Acids Res.*, **43**, W389-394.

640 38 Marsh, J.A., Singh, V.K., Jia, Z., Forman-Kay, J.D., (2006). Sensitivity of secondary structure
641 propensities to sequence differences between alpha- and gamma-synuclein: implications for
642 fibrillation. *Protein Sci.*, **15**, 2795-2804.

643 39 Sanfelice, D., Kelly, G., Curry, S., Conte, M.R., (2008). NMR assignment of the N-terminal
644 region of human La free and in complex with RNA. *Biomol NMR Assign*, **2**, 107-109.

645 40 Cruz-Gallardo, I., Martino, L., Kelly, G., Atkinson, R.A., Trotta, R., De Tito, S. *et al.*, (2019).
646 LARP4A recognizes polyA RNA via a novel binding mechanism mediated by disordered
647 regions and involving the PAM2w motif, revealing interplay between PABP, LARP4A and
648 mRNA. *Nucleic Acids Res.*, **47**, 4272-4291.

649 41 Cash, D.D., Feigon, J., (2017). Structure and folding of the Tetrahymena telomerase RNA
650 pseudoknot. *Nucleic Acids Res.*, **45**, 482-495.

651 42 Berman, A.J., Gooding, A.R., Cech, T.R., (2010). Tetrahymena telomerase protein p65 induces
652 conformational changes throughout telomerase RNA (TER) and rescues telomerase reverse
653 transcriptase and TER assembly mutants. *Mol. Cell. Biol.*, **30**, 4965-4976.

654 43 Podlevsky, J.D., Bley, C.J., Omana, R.V., Qi, X., Chen, J.J., (2008). The telomerase database.
655 *Nucleic Acids Res.*, **36**, D339-343.

656 44 Singh, M., Choi, C.P., Feigon, J., (2013). xRRM: a new class of RRM found in the telomerase
657 La family protein p65. *RNA biology*, **10**, 353-359.

658 45 Richards, R.J., Wu, H., Trantirek, L., O'Connor, C.M., Collins, K., Feigon, J., (2006). Structural
659 study of elements of Tetrahymena telomerase RNA stem-loop IV domain important for
660 function. *RNA*, **12**, 1475-1485.

661 46 Stefano, J.E., (1984). Purified lupus antigen La recognizes an oligouridylate stretch common
662 to the 3' termini of RNA polymerase III transcripts. *Cell*, **36**, 145-154.

663 47 Dock-Bregeon, A.C., Lewis, K.A., Conte, M.R., (2021). The La-related proteins: structures and
664 interactions of a versatile superfamily of RNA-binding proteins. *RNA biology*, **18**, 178-193.

665 48 Mastronarde, D.N., (2005). Automated electron microscope tomography using robust
666 prediction of specimen movements. *J. Struct. Biol.*, **152**, 36-51.

667 49 Zheng, S.Q., Palovcak, E., Armache, J.P., Verba, K.A., Cheng, Y., Agard, D.A., (2017).
668 MotionCor2: anisotropic correction of beam-induced motion for improved cryo-electron
669 microscopy. *Nat Methods*, **14**, 331-332.

670 50 Rohou, A., Grigorieff, N., (2015). CTFFIND4: Fast and accurate defocus estimation from
671 electron micrographs. *J. Struct. Biol.*, **192**, 216-221.

672 51 Zivanov, J., Nakane, T., Forsberg, B.O., Kimanius, D., Hagen, W.J., Lindahl, E. *et al.*, (2018).
673 New tools for automated high-resolution cryo-EM structure determination in RELION-3.
674 *Elife*, **7**.

675 52 Rosenthal, P.B., Henderson, R., (2003). Optimal determination of particle orientation,
676 absolute hand, and contrast loss in single-particle electron cryomicroscopy. *J. Mol. Biol.*, **333**,
677 721-745.

678 53 Kucukelbir, A., Sigworth, F.J., Tagare, H.D., (2014). Quantifying the local resolution of cryo-
679 EM density maps. *Nat Methods*, **11**, 63-65.

680 54 Emsley, P., Lohkamp, B., Scott, W.G., Cowtan, K., (2010). Features and development of Coot.
681 *Acta Crystallogr D Biol Crystallogr*, **66**, 486-501.

682 55 Pettersen, E.F., Goddard, T.D., Huang, C.C., Couch, G.S., Greenblatt, D.M., Meng, E.C. *et al.*,
683 (2004). UCSF Chimera-a visualization system for exploratory research and analysis. *J.*
684 *Comput. Chem.*, **25**, 1605-1612.

685 56 Song, Y., DiMaio, F., Wang, R.Y., Kim, D., Miles, C., Brunette, T. *et al.*, (2013). High-resolution
686 comparative modeling with RosettaCM. *Structure*, **21**, 1735-1742.

687 57 Adams, P.D., Afonine, P.V., Bunkoczi, G., Chen, V.B., Davis, I.W., Echols, N. *et al.*, (2010).
688 PHENIX: a comprehensive Python-based system for macromolecular structure solution. *Acta*
689 *Crystallogr D Biol Crystallogr*, **66**, 213-221.

690 58 Croll, T.I., (2018). ISOLDE: a physically realistic environment for model building into low-
691 resolution electron-density maps. *Acta Crystallogr D Struct Biol*, **74**, 519-530.

692 59 Williams, C.J., Headd, J.J., Moriarty, N.W., Prisant, M.G., Videau, L.L., Deis, L.N. *et al.*, (2018).
693 MolProbity: More and better reference data for improved all-atom structure validation.
694 *Protein Sci.*, **27**, 293-315.

695 60 Guillerez, J., Lopez, P.J., Proux, F., Launay, H., Dreyfus, M., (2005). A mutation in T7 RNA
696 polymerase that facilitates promoter clearance. *Proc Natl Acad Sci U S A*, **102**, 5958-5963.
697 61 Wang, Y., Yesselman, J.D., Zhang, Q., Kang, M., Feigon, J., (2016). Structural conservation in
698 the template/pseudoknot domain of vertebrate telomerase RNA from teleost fish to human.
699 *Proc Natl Acad Sci U S A*, **113**, E5125-5134.

700 **Table 1: Binding affinity of p65 and TER constructs determined from EMSA experiments.**

Protein	RNA	Kd* (nM)	Relative Kd
αN-LaMod(67-355) LaMod(108-355)	S1hp-S4hp	530±50	~1.2
		646±16	
αL-xRRM2 xRRM2	SL4	816±57	~1.6
		1319±102	
αL-xRRM2	SL4	816±57	—
	SL4ΔU	848±71	

*Determined Kds are average of three experiments.

FIGURES

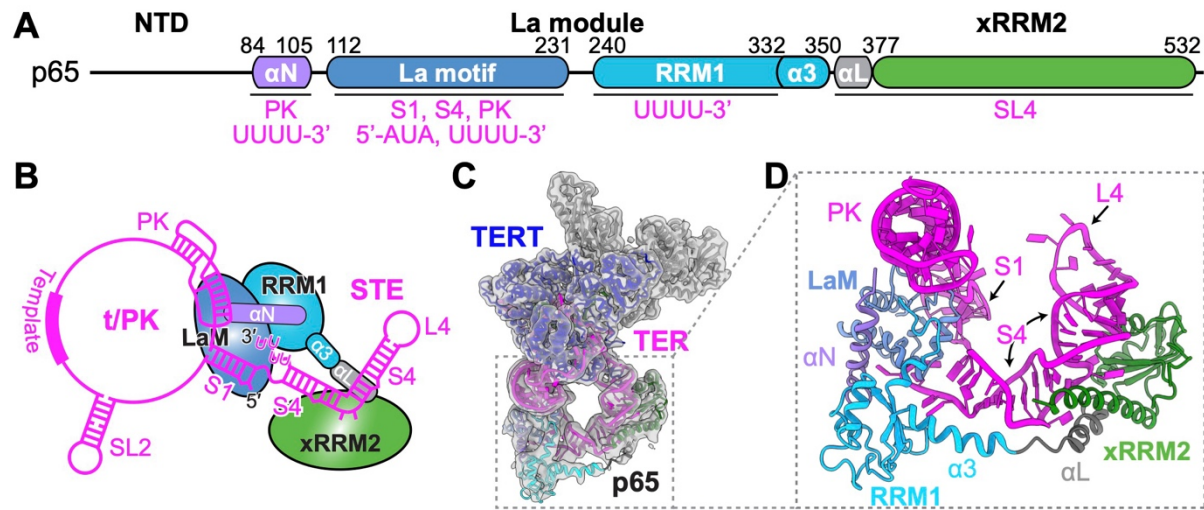


Figure 1: Structure of p65–TER complex in *Tetrahymena* telomerase. **(A)** Schematic of determined domain structure of p65, including newly identified helices α N, RRM1 α 3, and α L, and corresponding TER interacting regions. **(B)** Schematic of the secondary structure of TER and binding sites for p65 NTD, LaM, RRM1, and xRRM2 (shown schematically). **(C)** Cryo-EM density map of *Tetrahymena* telomerase at 3.8 Å resolution with improved density for the p65-TER region. **(D)** Molecular model of p65–TER complex in telomerase. Newly identified helices α N, RRM1 α 3, and α L are labeled. Coloring scheme for p65 is α N (violet), LaM (blue), RRM1 including α 3 (cyan), α L (gray), xRRM2 (green), and TER is magenta.

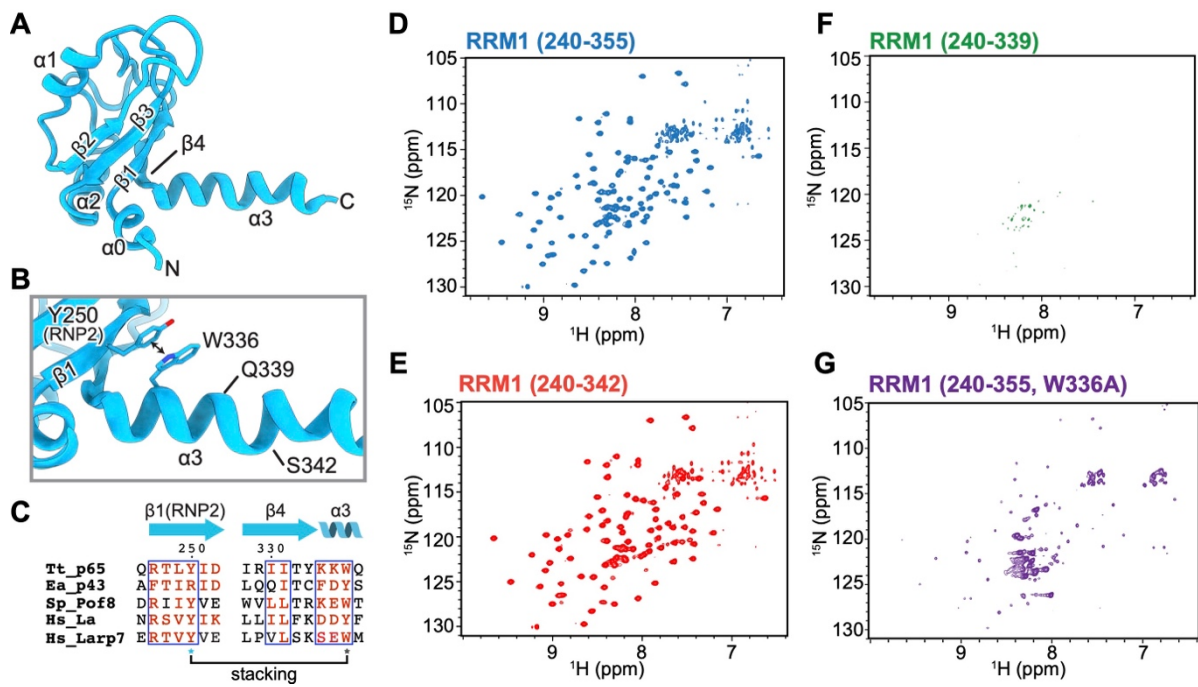


Figure 2: Structure and stability of La Module RRM1. (A) Structure of RRM1 including non-canonical helices α 0 and α 3. (B) Region of RRM1 showing stacking interaction between Y250 on β 1 and W336 on α 3. (C) Sequence alignment of β 1 and α 3 from various LARP7 proteins (Tt, *Tetrahymena*; Ea, *Euplotes aediculatus*; Sp, *Schizosaccharomyces pombe*; Hs, *Homo sapiens*). (D-G) ^1H - ^{15}N HSQC spectra of RRM1 constructs: (D) RRM1(240-355), (E) RRM1(240-342), (F) RRM1(240-339), (G) RRM1(240-355, W336A).

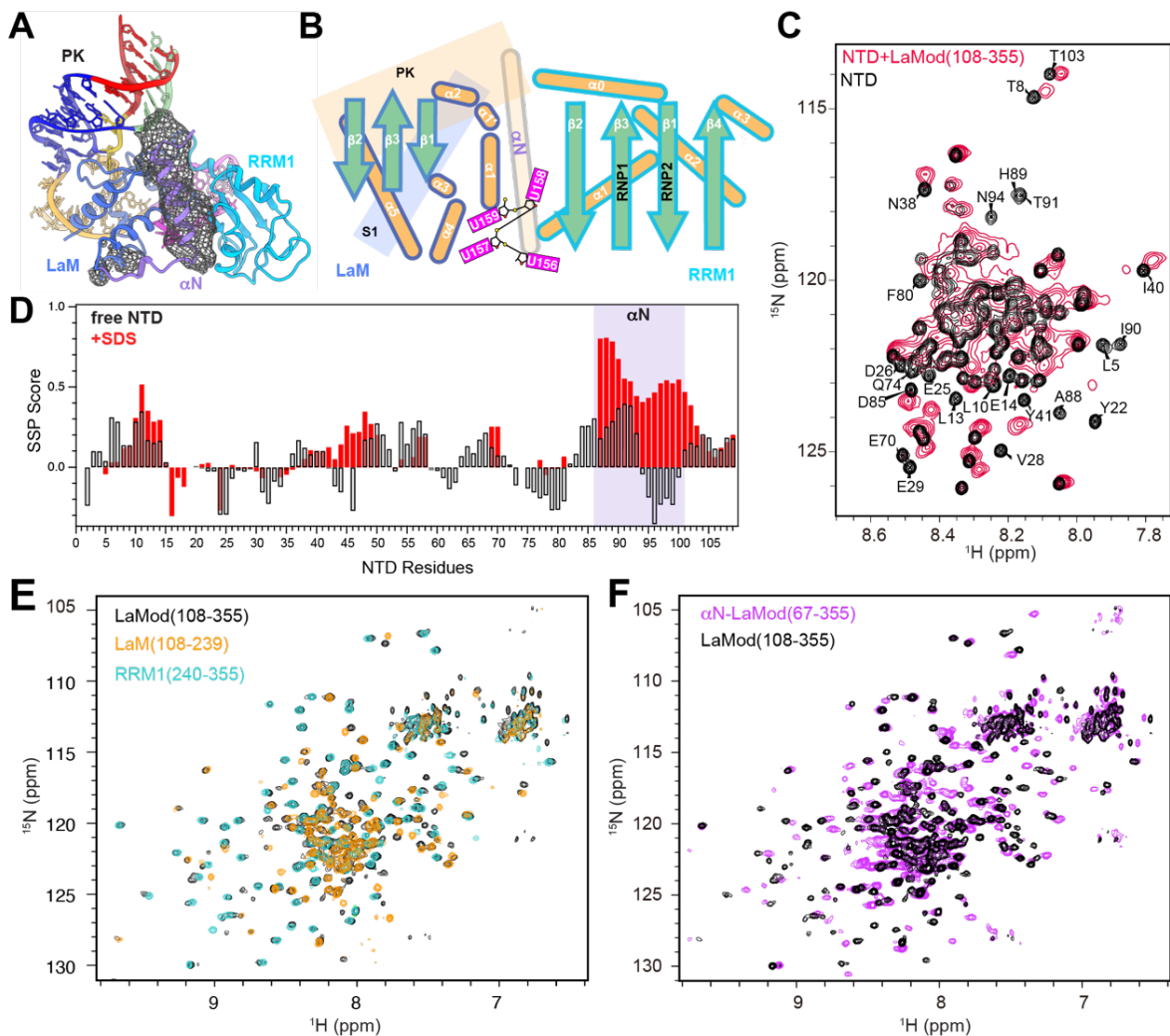


Figure 3: p65 NTD αN binds the La module **(A)** Model of La module with TER, with cryo-EM density between LaM and RRM1 that was assigned to NTD αN shown as mesh surface. **(B)** Schematic representation of secondary structure elements of La module LaM and RRM1 and interactions with PK, S1, and UUUU-3'-OH. **(C)** ^1H - ^{15}N HSQC spectra of ^{15}N -labeled NTD (1-109) in the absence (black) and presence of LaMod(108-355) (red). See Supplementary Figure S3 for sequence and S4 for amide assignments. The peaks in the free NTD that are perturbed in the complex are labeled. **(D)** Secondary Structure Propensity (SSP) Score of p65 NTD in 25mM SDS. +1 means 100% population of α -helical conformation and -1 means 100% population of β -strand conformation. **(E)** ^1H - ^{15}N HSQC spectra of p65 ^{15}N -labeled LaM (orange), RRM1 (cyan) and LaMod(108-355) (black). **(F)** ^1H - ^{15}N HSQC spectra of p65 ^{15}N -labeled LaMod(108-355) (black) and αN -LaMod(67-355) (purple).

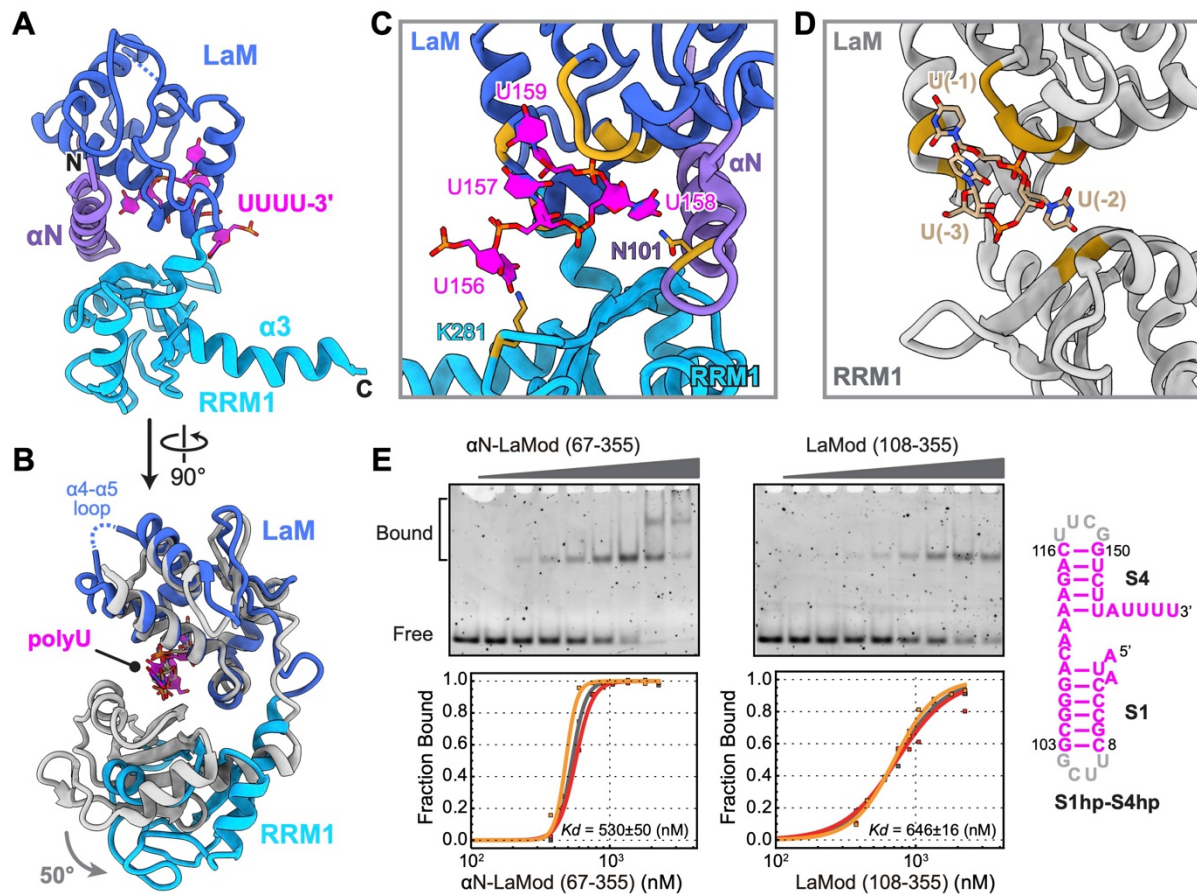


Figure 4: Interactions between p65 and the polyU tail of TER. (A) Model of p65 αN-La module with UUUU-3'. (B) Superposition of La modules of p65 (colored) and La protein (gray, PDB ID 2VOO) in complex with polyU tail highlighting the more open form of p65 due to αN interaction. p65 RRM1 α3 and αN, which are not present in the La protein structure, are omitted for clarity. (C) Locations of UUUU-3' on p65 LaM, RRM1, and αN and potential interactions. (D) Locations of UUU-3' on La protein La module (PDB ID 2VOO). Colors are as in Figure 1. (E) Representative EMSA of αN-LaMod (left) and LaMod (right) and corresponding binding curves from 3 experiments. For each sample, the concentration of S1hp-S4hp was 100 nM, and the protein concentration was increased stepwise from 375 to 2250 nM. Sequence and secondary structure of RNA (S1hp-S4hp) used in the EMASAs is shown at far right. Gray nucleotides are non-native sequence.

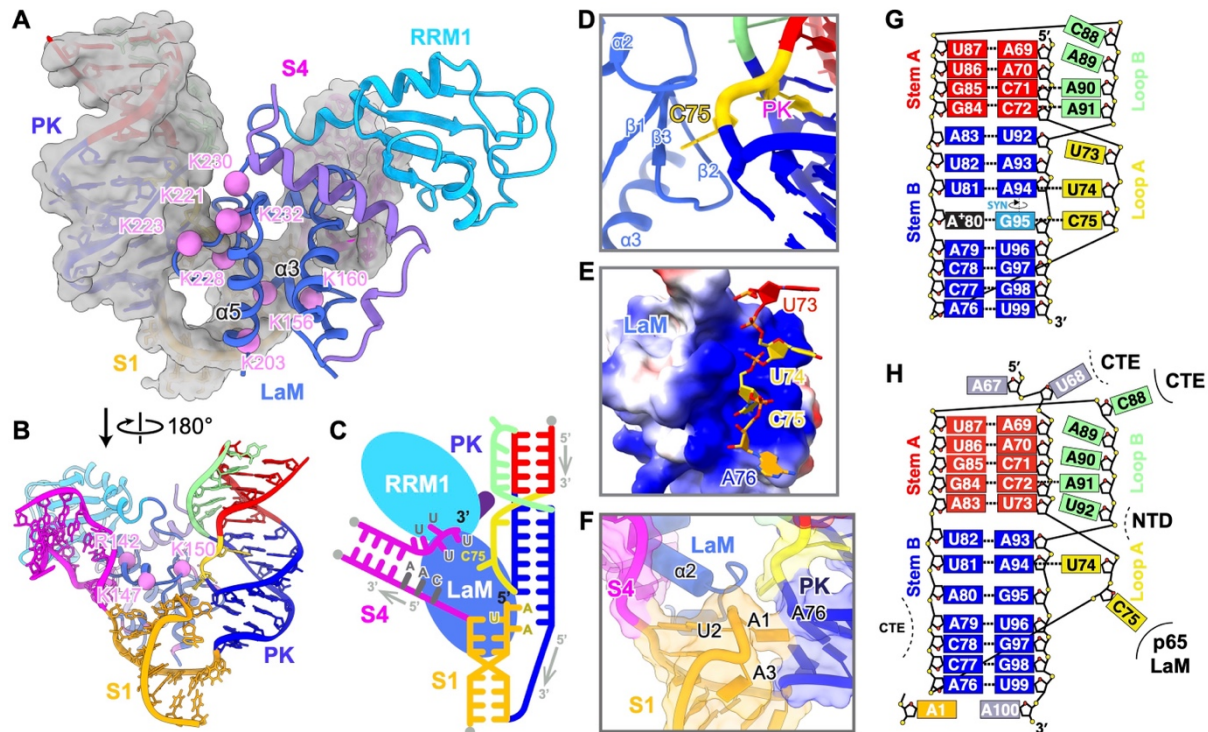
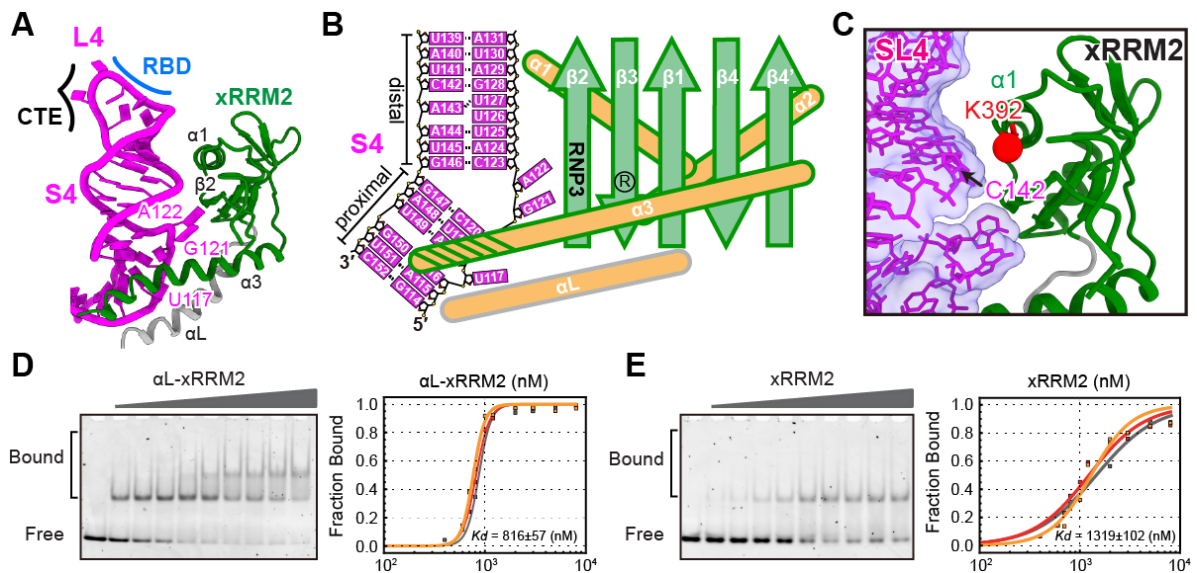


Figure 5: p65 α N-LaM binds the TER 5'-end, UUUU-3'-OH, and PK. (A) The interactions between α N-LaM (shown as ribbon) and S1, PK and S4 (shown as sticks inside surface). Positively charged residues located on LaM–PK and LaM–S1 interfaces are shown as pink spheres. **(B)** 180° rotation of (A) showing additional positively charged residues from LaM that contact S1, S4, and the 5' end. **(C)** Schematic of α N-La module interactions with TER. **(D)** PK loop residue C75 inserts into a groove between LaM β 2 and β 3 (left). **(E)** 90° rotation of (D) showing PK loop residues 73-76 backbones in the basic groove on LaM. LaM is shown as a grasp surface. **(F)** Region of LaM at intersection of PK, S1, and S4 shows that LaM α 2 stacks on the terminal base pair of S1 and 5'-end nucleotide A1 of TER stacks underneath PK. **(G,H)** Schematics of PK secondary structures without p65 in solution determined by NMR (F) and in telomerase by cryo-EM (G). The domains of p65 and TERT contacting PK nucleotides are annotated in G. Solid and dashed lines by protein domain names indicate base and backbone interactions, respectively.



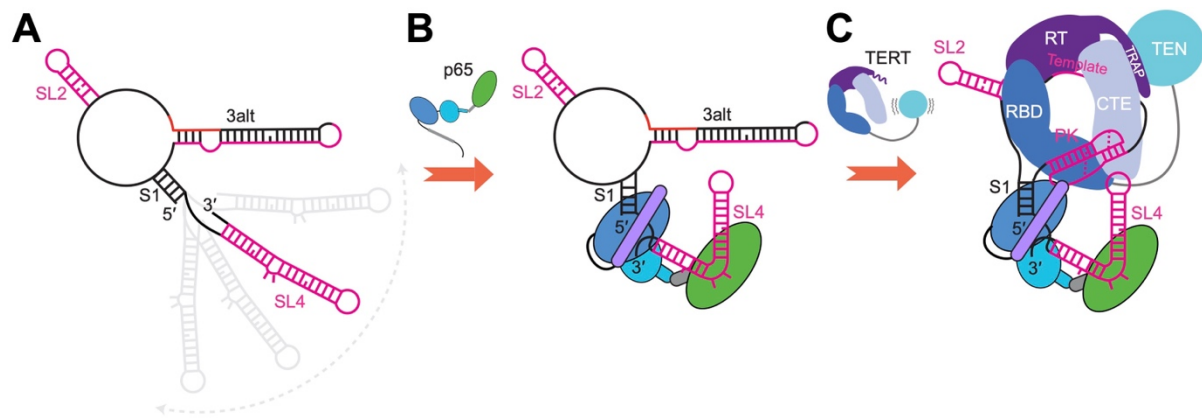


Figure 7: Steps in p65-TER-TERT assembly. **A.** Secondary structure of free TER based on NMR data (54). The t/PK of free TER forms stem 3alt, sequestering the residues that form the PK. STE SL4 is connected stem 1, which closes the t/PK circle, through a short single-stranded linker (CAA). Gray shadows indicate that its position is not fixed relative to the t/PK. **B.** p65 α N-La module binds S1 and UUUU-3'-OH while α L-xRRM2 binds and bends SL4. **C.** The assembled p65-TER-TERT complex. p65 orients SL4 to insert into the RBD-CTE interface to lock the TERT ring, and α N-La module interacts with stem 1, UUUU-3'OH, and PK. α N-La module may facilitate formation of the PK and/or stabilization of its interaction with TERT.

SUPPLEMENTARY INFORMATION

Table S1: Cryo-EM data collection, refinement and validation statistics

Sample	p65 of <i>Tetrahymena</i> telomerase
EMDB ID	EMD-29903
PDB ID	8GAP
Data collection and processing	
Magnification	105,000
Voltage (kV)	300
Electron exposure (e-/Å ²)	48
Defocus range (μm)	-0.8 – -4.0
Pixel size (Å)	1.36
Symmetry imposed	C1
Initial particle images (no.)	7,768,528
Particles after initial screening (no.)	954,244
Final particle images (no.)	162,358
Map resolution (Å)	3.8
FSC threshold	0.143
Map resolution range (Å)	3.5 – 6.5
Refinement	
Initial model used (PDB code)	7UY6
Model resolution (Å)	4.0
FSC threshold	0.5
Map sharpening <i>B</i> factor (Å ²)	-82.0
Model composition	
Non-hydrogen atoms	20,630
Protein residues	2,032
RNA/DNA Nucleotides	173
Ligands	1
<i>B</i> factors (Å ²)	
Protein	220.73
Nucleotides	264.06
R.m.s. deviations	
Bond lengths (Å)	0.003
Bond angles (°)	0.862
Validation	
MolProbity score	1.86
Clashscore	12.59
Poor rotamers (%)	0.21
Ramachandran plot	
Favored (%)	96.27
Allowed (%)	3.68
Disallowed (%)	0.05

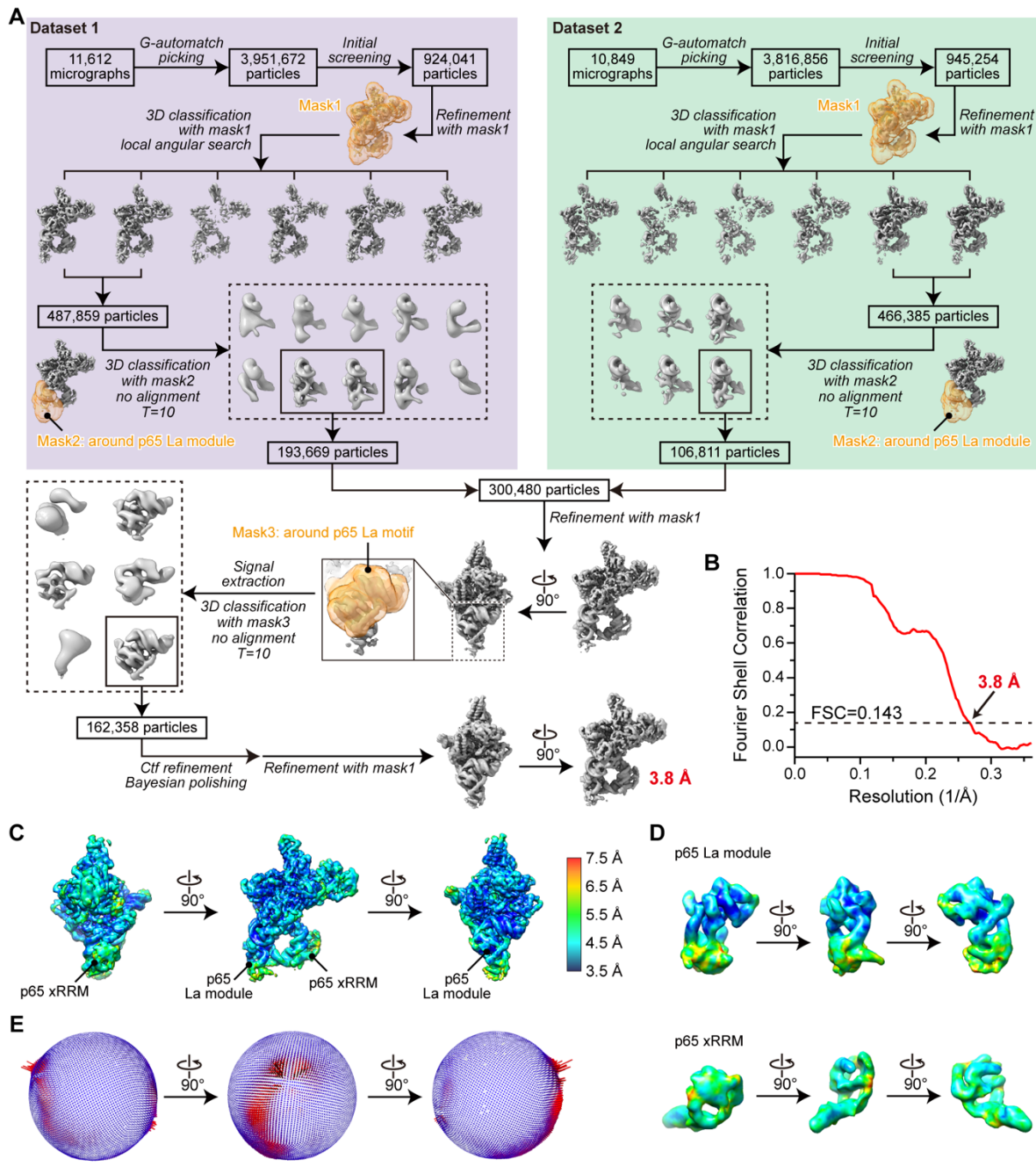


Figure S1: Cryo-EM data processing workflow of *Tetrahymena* p65-TER complex. (A) Data processing workflow (detailed in methods). Soft masks used in data processing are colored in orange. **(B)** Plot of the Fourier shell correlation (FSC) as a function of the spatial frequency with resolution of the final reconstruction indicated. **(C,D)** Surface views of local resolution evaluation of the 3.8 Å-resolution cryo-EM map of the entire catalytic core **(C)** and p65 subdomains **(D)**. **(E)** Euler angle distributions of telomerase particles used for the 3.8 Å-resolution reconstruction.

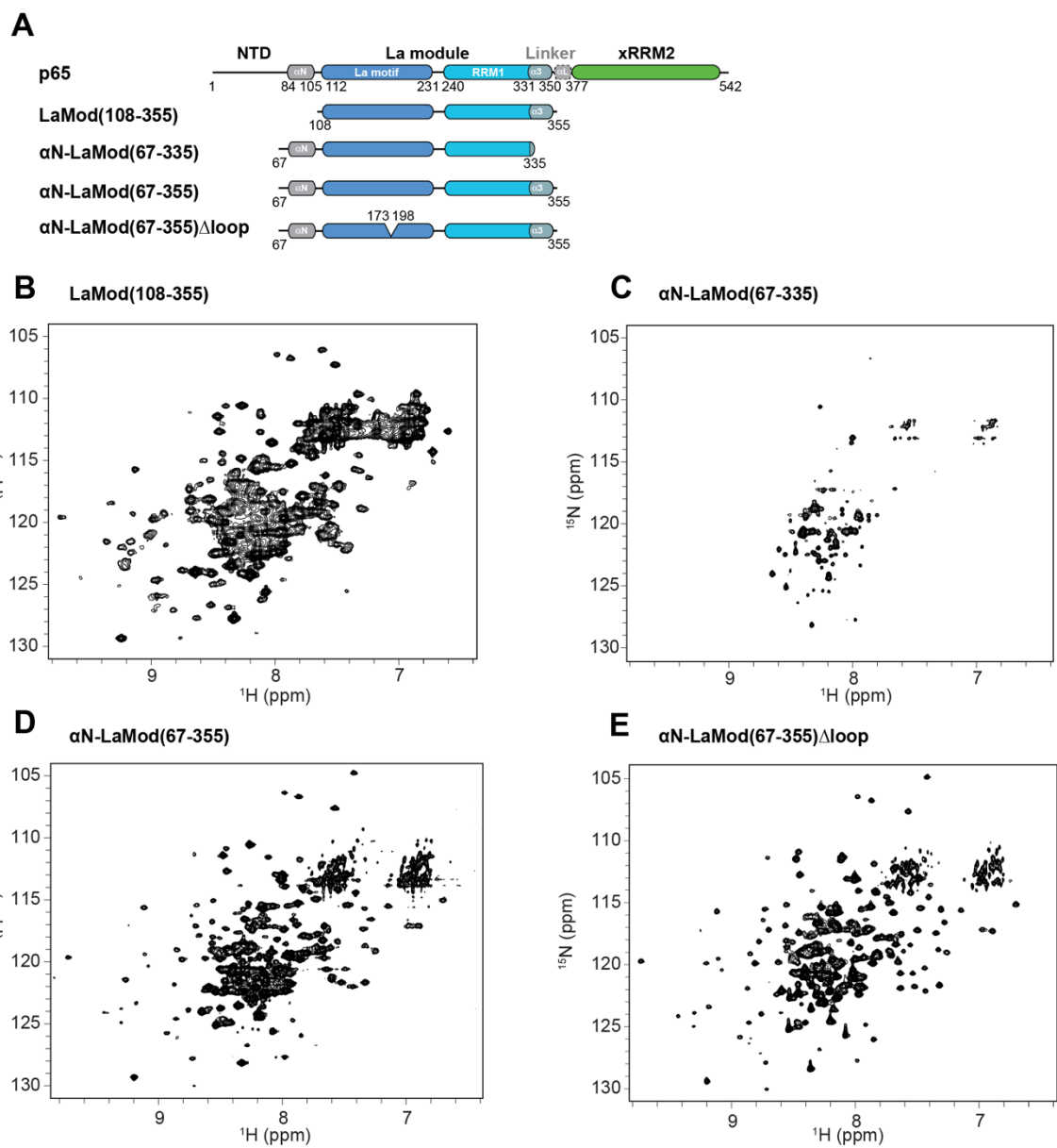


Figure S2: La module constructs of *Tetrahymena* p65. (A) Domain structure of p65 and p65 La module constructs. **(B-E)** ^1H - ^{15}N HSQC spectra of p65 La module constructs shown in (A).

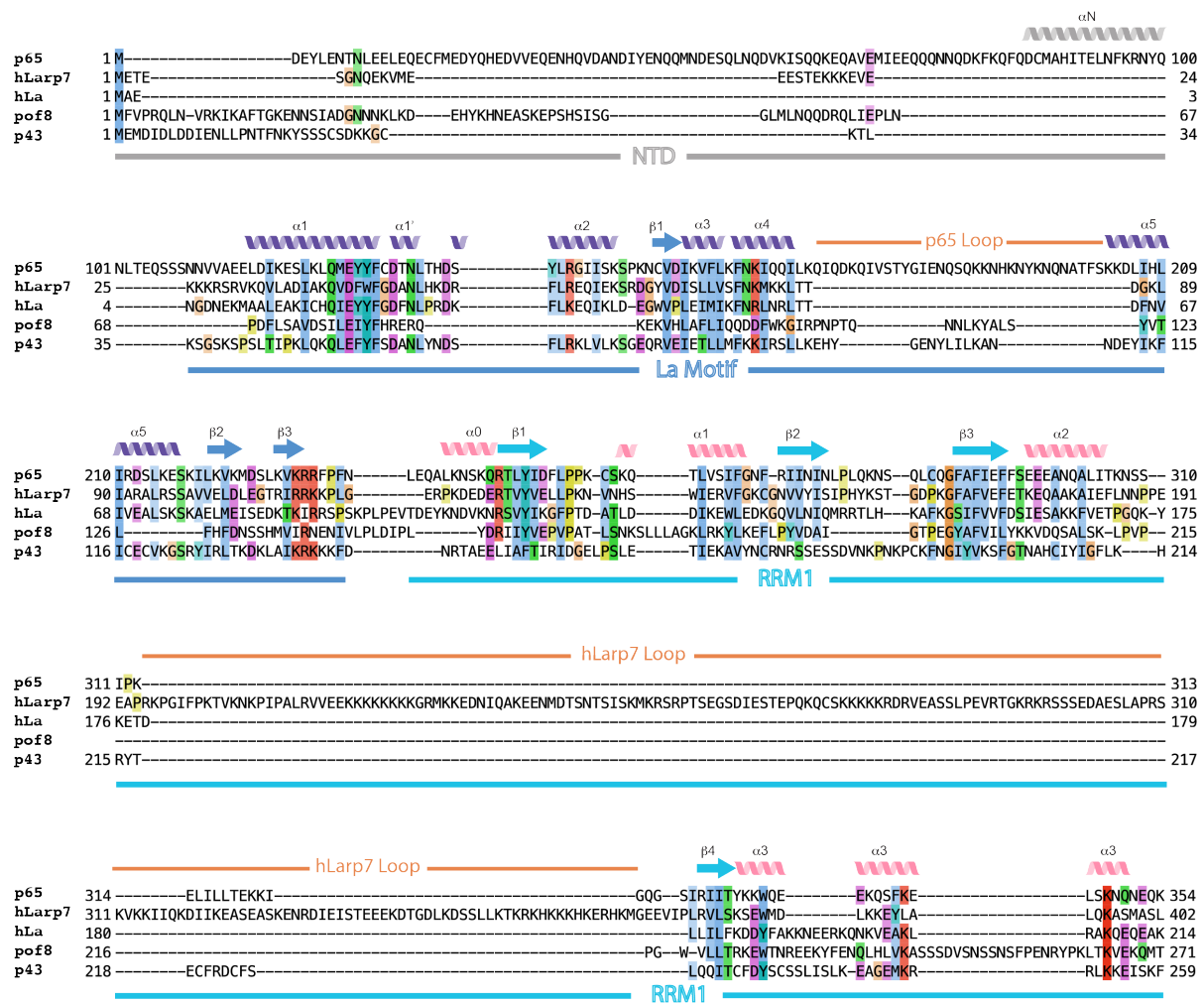


Figure S3: Sequence alignment of La modules from LARP7 and human genuine La proteins.

Secondary structures of *Tetrahymena* p65 La module are shown on top. p65, *Tetrahymena* p65; hLarp7, human Larp7; hLa, human genuine La protein; pof8, fission yeast pof8; p43, *Euplotes* p43.

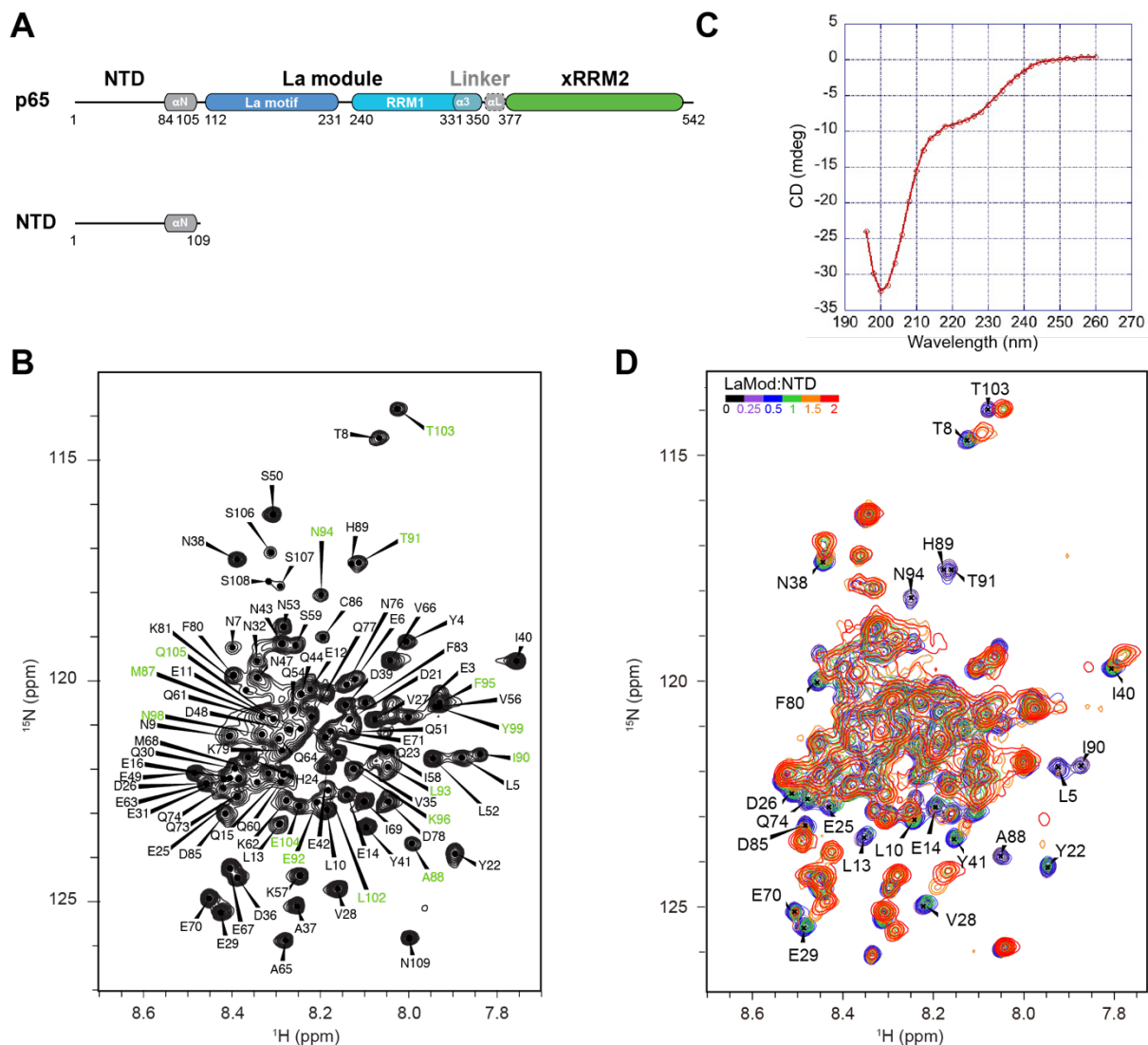


Figure S4: p65 NTD is an intrinsically disordered region that forms a C-terminal helix α N in complex with La module. (A) Domain structure of p65 and p65 NTD. **(B)** ^1H - ^{15}N HSQC spectrum of NTD. The helix α N residues are labeled in green. **(C)** CD spectrum of NTD, indicating it is intrinsically disordered. **(D)** ^1H - ^{15}N HSQC spectra of ^{15}N labeled NTD, free and with increasing amounts of unlabeled LaMod(108-355). The spectra with [NTD]:[LaMod(108-355)] concentration ratio 1:0, 1:0.25, 1:0.5, 1:1.0, 1:1.5, 1:2.0, are colored in black, purple, blue, green, orange and red, respectively, also shown as color key at the top of the spectra. The peaks that are shifted or disappear due to line broadening from chemical exchange in the presence of LaMod(108-355) are labeled on the free NTD spectrum.

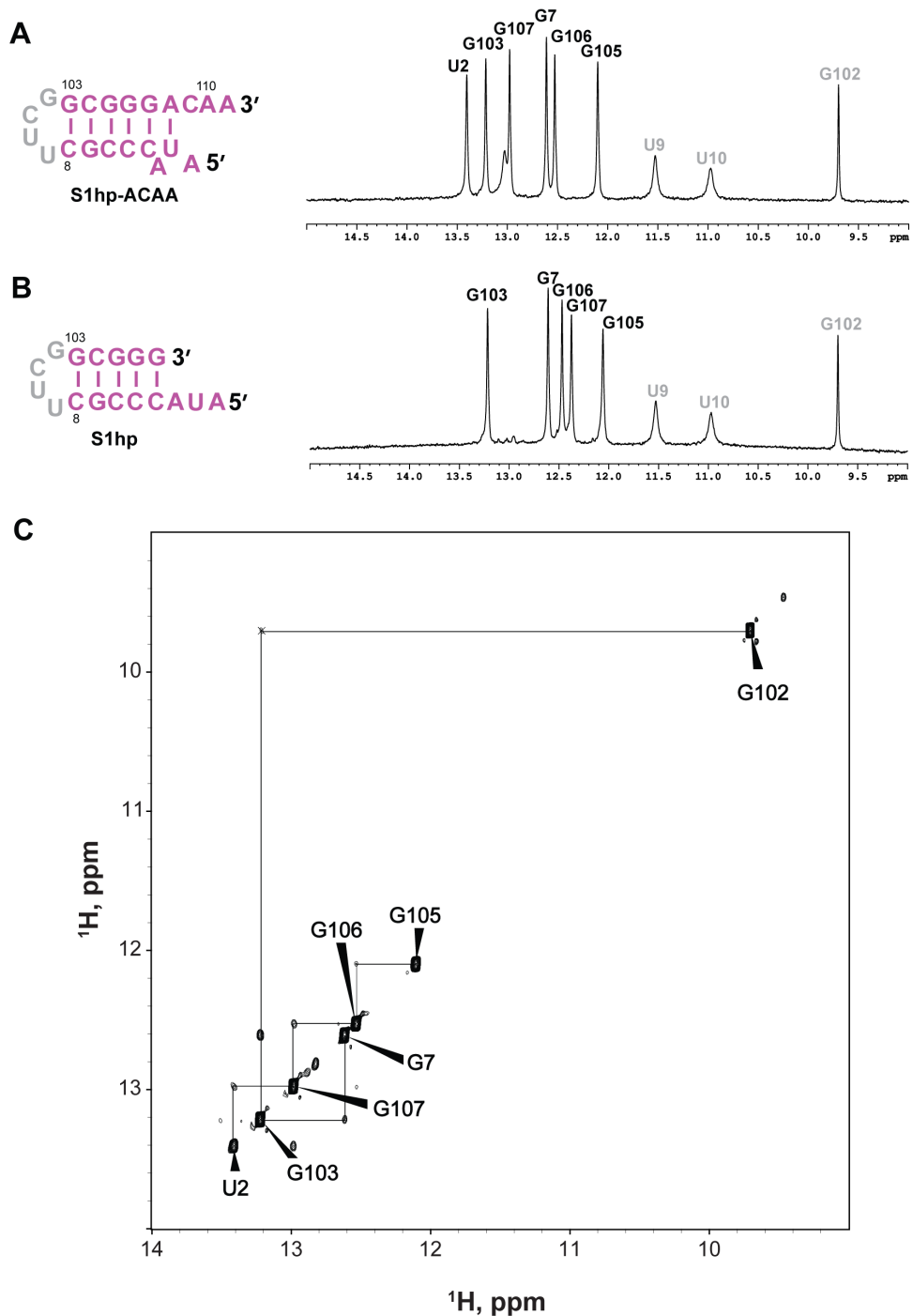


Figure S5: 800 MHz 1D imino proton and NOESY spectra of TER S1 hairpin constructs shows U2 pairs with A108 to extend stem 1 at 283 K. (A) RNA construct that contains S1 hairpin, ACAA108-111 linker and 5'-end (S1hp-ACAA). **(B)** RNA construct that contains S1 hairpin and 5'-end (S1hp). **(C)** Imino NOESY spectrum of S1hp-ACAA. The NMR buffer 10 mM sodium phosphate, pH 6.4, 50 mM KCl, 10% v/v D₂O. NOESY mixing time is 200 ms.

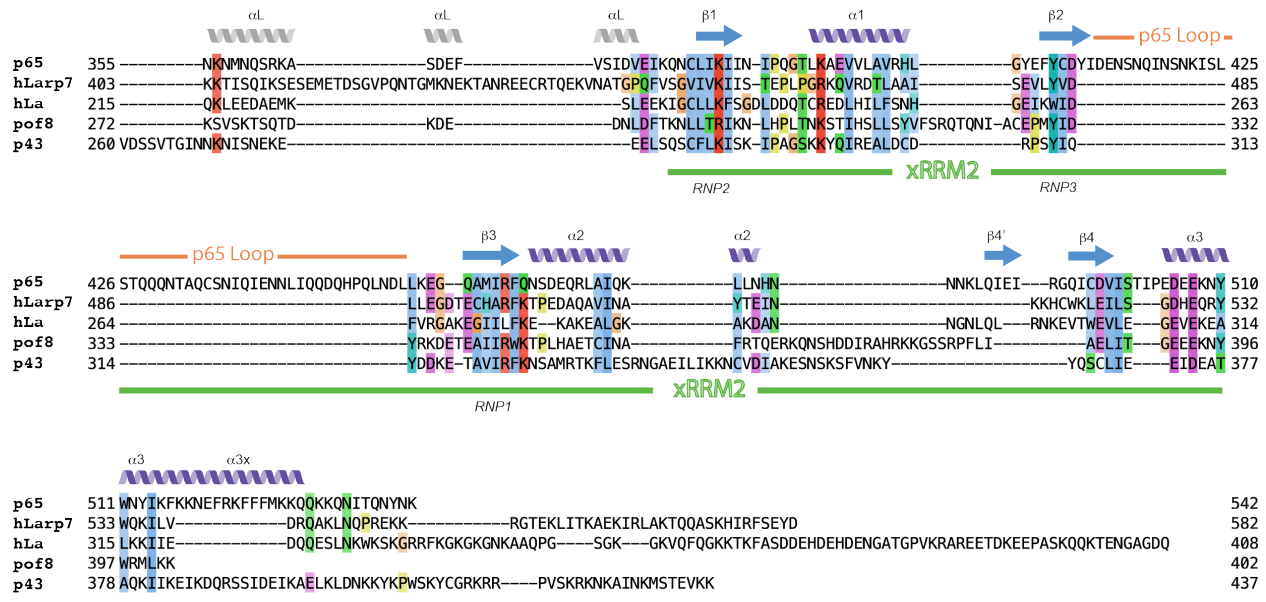


Figure S6: Sequence alignment of LARP7 and human genuine La xRRM2 domains. Secondary structures of *Tetrahymena* p65 xRRM2 are shown on top. p65, *Tetrahymena* p65; hLarp7, human Larp7; hLa, human genuine La protein; pof8, fission yeast pof8; p43, *Euplotes* p43.

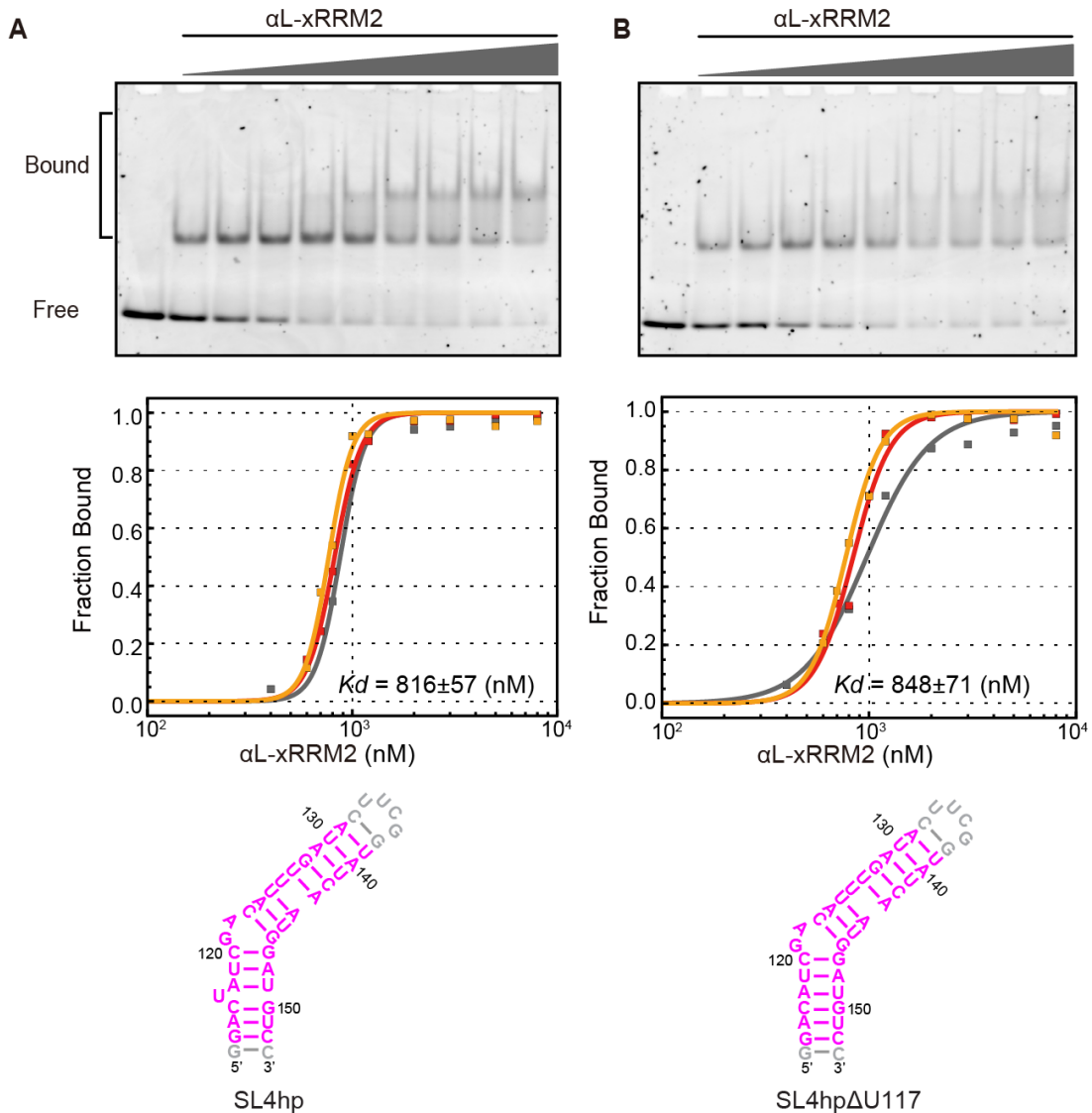


Figure S7: EMSAs of α L-xRRM2 with SL4hp and SL4hp Δ U117. Representative EMSA of α L-xRRM2 with SL4 (left) and SL4 Δ U (right) and corresponding binding curves from 3 experiments. The sequences and secondary structures of SL4 and SL4 Δ U used in the EMSAs are shown at the bottom. Gray nucleotides are non-native. For each sample, the concentration of RNA was 150 nM, and the protein concentration was increased stepwise from 600 to 8000 nM.

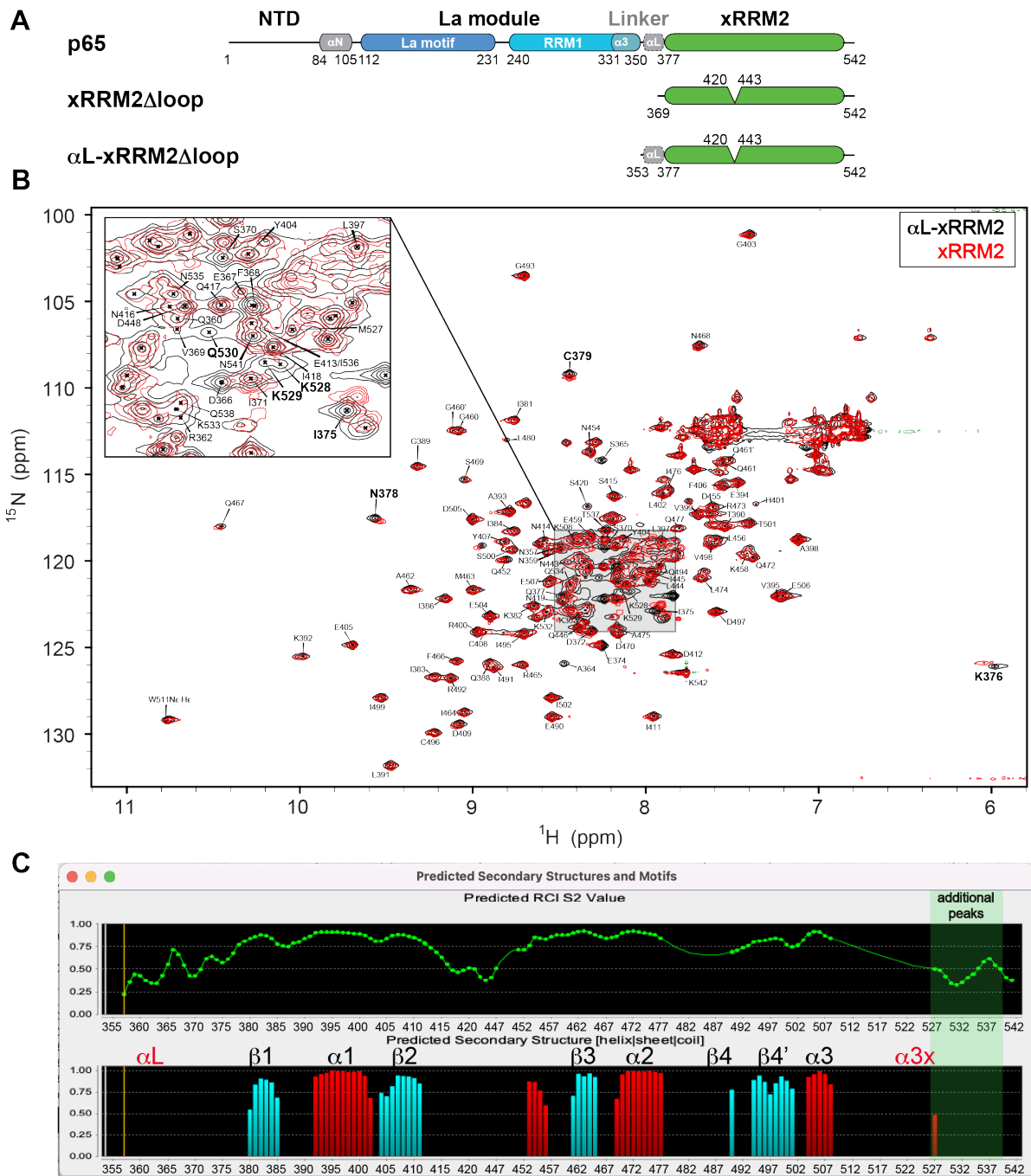


Figure S8: ^1H - ^{15}N HSQC spectra of p65 xRRM2. (A) Domain structure of p65 and xRRM2 constructs. Δloop is a partial truncation of $\beta 2$ - $\beta 3$ loop between (not including) residues 420 and 443, also shown on the cartoon diagrams. (B) ^1H - ^{15}N HSQC spectrum of p65-xRRM2 without helix αL (red) overlaid with p65- αL -xRRM2 (black). (C) TALOS-N analysis for p65- αL -xRRM2. Residues that had resonances in αL -xRRM2 but not in xRRM2 were highlighted in green shaded box.